Collision-induced Ramsey resonances in Sm vapor

E. Buhr
Institut für Quantenoptik, Universität Hannover, 3000 Hannover 1, Federal Republic of Germany

J. Mlynek
Institut für Quantenelektronik, Eidgenössische Technische Hochschule (ETH) Zürich, CH-8093 Zürich, Switzerland

(Received 12 March 1987)

We report detailed studies of Ramsey-type resonances due to collisional velocity diffusion of Sm atoms within the Doppler-broadened $^7F_1 \rightarrow {}^7F_0$ ^{154}Sm transition at $\lambda = 570.68$ nm in the presence of rare-gas perturbers (He,Ne,Ar,Kr,Xe). The experimental technique uses counterpropagating laser fields and relies on coherent resonance Raman processes to excite and detect sublevel coherence optically. A modulated pump laser field is used for velocity-selective resonance Raman excitation of oscillating Zeeman coherence in the $J=1$ ground state of Sm; the sublevel coherence is monitored by Raman heterodyne detection using a counterpropagating, unmodulated probe laser field. If the pump and probe fields interact with different atomic velocity subgroups, a signal only occurs in the presence of velocity-changing collisions which provide a transport of the Sm atoms with sublevel coherence in velocity space. The sublevel resonance curves turn out to be sensitive to both depolarizing and velocity-changing collisions; the measured line shapes show the characteristic features of Ramsey-type resonances. Our theoretical treatment is based on a novel four-level density matrix calculation; the analysis reveals that the temporal evolution of the collisional velocity-diffusion processes can simply be obtained by means of a Fourier transformation of the measured sublevel resonance curves. In the case of He perturbers the diffusion in velocity space can be described by a Fokker-Planck equation; here, the theoretical fits of the measured sublevel resonance curves directly yield the time constant for collisional thermalization and the cross section for depolarizing collisions. In the case of the heavier rare gases, however, the Fokker-Planck model fails to describe the velocity thermalization; here, the Keilson-Storer kernel yields a better agreement with the experimental data. We derive cross sections for depolarizing and velocity-changing collisions and values for the collisional velocity changes associated with orientation-preserving collisions.

I. INTRODUCTION

In the "classical" Ramsey-resonance method two spatially separated radio-frequency (rf) fields are used in atomic and molecular beam experiments for the observation of narrow rf resonances.[1] Recently, the observation of Ramsey fringes was reported also for a resonantly driven Raman transition;[2] here, the two separated rf fields were replaced by two modulated laser fields in order to create sublevel coherence in a Λ-folded three-level system. In a more recent atomic-beam experiment Ramsey fringes were observed for a resonance Raman transition even without applying a second "oscillatory" field.[3] Again a modulated laser field was used for coherent Raman excitation of sublevel coherence; the required phase-sensitive detection, however, was achieved by Raman heterodyne detection[4,5] of the atomic coherence using a spatially separated but unmodulated probe laser field. This coherent detection scheme is exclusively sensitive to oscillating sublevel coherence, and thus an essentially background-free observation of the Ramsey resonances can be obtained. Let us also point out that this coherent Raman Ramsey method for the observation of optically induced rf Ramsey resonances is based on the creation and detection of *sublevel coherence;* in this respect it is far different from Ramsey resonance methods concerning the optical frequency region.[6]

This particular excitation and detection scheme of Raman heterodyne Ramsey spectroscopy also offers the opportunity to extend the Ramsey-resonance idea into a domain that is substantially different from other Ramsey-resonance experiments considered so far. We recently reported in brief on the observation of Ramsey fringes due to collisional velocity diffusion in an atomic vapor. Here, the experimental technique uses counterpropagating laser fields and relies on coherent resonance Raman processes to optically excite and detect sublevel coherence within a *Doppler-broadened atomic transition;* in this experiment the occurrence of the Ramsey fringes results from the "motion" of atoms with sublevel coherence between two interaction zones separated in "velocity" space rather than in "local" space.[7]

It is the aim of this paper to relate a number of details to the experimental observation and theoretical description of this novel phenomenon. As the Ramsey resonance only occurs in the presence of velocity-changing collisions (VCC), it has been called "collision-induced Ramsey resonance."[7] We especially analyze the potential of this method to study collisional-redistribution processes in atomic vapors.[8] It will be shown that this

method indeed provides a new way to monitor the effects of both depolarizing and velocity-changing collisions associated with atomic multipole components in a J-state manifold; out of the steady-state experimental data even the *temporal evolution* of the velocity-diffusion processes can be extracted, thus permitting novel insights into the nature of the collisional relaxation and redistribution of specific anisotropic moments. In this way our technique supplements the various other laser spectroscopic methods like polarization spectroscopy[9–12] or photon-echo experiments[13–14] that already have been applied to the study of VCC concerning multipole moments such as orientation and alignment.

For our studies we consider an inhomogeneously broadened, Zeeman-split $J=1-J'=0$ transition and investigate the collisional relaxation and redistribution of the transverse orientation in the $J=1$ ground state. This atomic-model system is not only relatively simple in its theoretical treatment, but above all it is experimentally accessible. Thus a direct comparison of experimental and theoretical line shapes becomes possible, which in principle allows a determination of the theoretical model parameters characterizing the atomic collision processes. In particular, velocity-thermalization rates and cross sections for depolarizing collisions can be obtained from our experiments. We will also show that it is possible to gain information on the rates and velocity changes associated with atomic collisions that preserve the transverse orientation in the studied $J=1$ ground state of Sm.

The structure of our paper is as follows. To start with, we briefly explain the basic idea of our experimental technique. In Sec. III a theoretical description of the Ramsey-resonance formation is given. The experimental results are presented in Sec. IV, and in Sec. V we discuss the measured data such as collisional parameters and compare them with the theoretical predictions.

II. PRINCIPLE OF EXPERIMENT

The Ramsey-resonance experiment discussed in this paper is performed in an atomic vapor, in which two counterpropagating laser fields, the modulated pump and the unmodulated probe laser field, spatially overlap [see Fig. 1(e)]. The spectral components of the modulated pump laser field (carrier of frequency ω_E and modulation sidebands of frequencies $\omega_E \pm \omega_M$) couple three Zeeman sublevels of a long-lived, Zeeman-split $J=1$ ground state to a common optically excited state with $J'=0$ [see Fig. 1(a)]. In a resonant-Raman process a coherence between the Zeeman sublevels is created. This excitation scheme of sublevel coherence is inherently Doppler-free, independent from the width of the homogeneous optical linewidth and is, moreover, insensitive to laser frequency jitter.[2,4]

In the case of a Doppler-broadened optical transition and for narrow-bandwidth laser excitation the sublevel coherence is excited in a single atomic velocity subgroup, whose width in velocity space is determined by the homogeneous optical linewidth Γ [see Fig. 1(d)]. Thus, for a given laser frequency detuning Δ_E with respect to the center of the Doppler profile a sublevel coherence is created by the modulated pump field in atoms with a velocity centered around $\Delta_E/k \equiv -v_0$. In contrast, the counterpropagating probe beam, which is used for Raman heterodyne detection of the sublevel coherence, interacts with atoms having the opposite velocity $+v_0$. The probe beam is therefore only capable of detecting the sublevel coherence in the velocity interval centered around $+v_0$ [see Fig. 1(d)]; hence, for a nonzero laser frequency detuning ($\Delta_E \neq 0$) a signal is achieved only if the active atoms change their velocity from $-v_0$ to $+v_0$, i.e., if they "move" in velocity space.

One well-known mechanism that provides velocity changes in a vapor are collisions that preserve the internal atomic state.[8] Here we consider velocity-changing collisions of the active atoms with added rare-gas perturbers. Especially in the case of light perturbers, the active atoms perform a Brownian motion in velocity space.[15] During this collisional redistribution from the velocity $-v_0$ to other velocities the active atoms are not affected by the laser fields due to the Doppler effect; as a consequence, the sublevel coherence evolves at its eigenfrequency Ω_M [see Fig. 1(b)] and a phase shift between the sublevel coherence and the oscillatory laser modulation of frequency ω_M is built up.

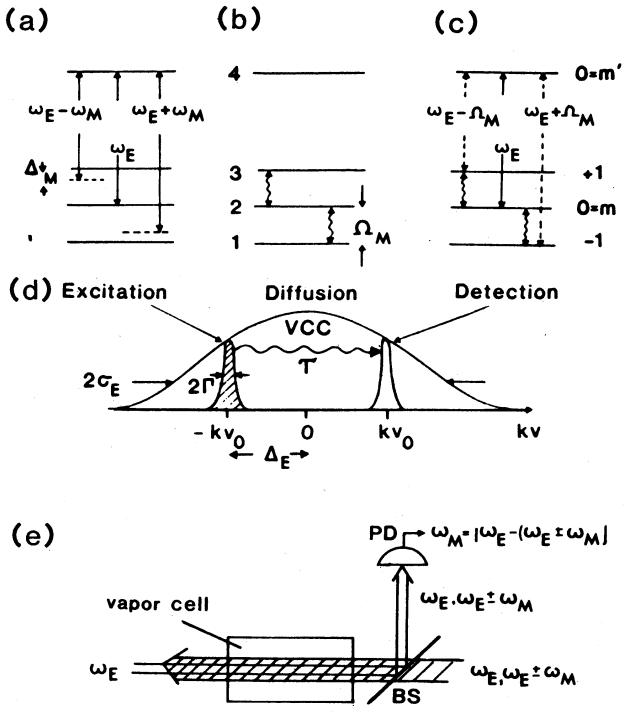

FIG. 1. (a) Modulated excitation process of Zeeman coherence for a nondegenerate $J=1-J'=0$ transition; (b) free evolution of sublevel coherence during velocity diffusion; (c) detection process showing Raman sidebands; (d) outline of the velocity selectivity of the excitation and detection of sublevel coherence in a Doppler-broadened optical transition; (e) experimental scheme for the observation of collision-induced Ramsey resonances in Sm vapor: BS, beam splitter; PD, photodetector.

In order to explain the Ramsey-resonance formation, let us assume that at a certain time $t=t_0$ an active atom has been pushed out of the initially excited velocity subgroup centered around $v=-v_0$. Since the sublevel coherence between the $|\Delta m|=1$ Zeeman substates is driven by the modulated pump laser field at frequency ω_M, the sublevel coherence exhibits a phase factor given by $\exp(\pm i\omega_M t_0)$; the plus and minus sign is related to the sublevel coherence ρ_{12} and ρ_{32}, respectively (see level scheme in Fig. 1). As has been discussed above, during the velocity-diffusion process the coherence evolves at its eigenfrequency Ω_M. If the active atom accidentally "arrives" after a certain time $\tau=t-t_0$ in the atomic subgroup with the velocity $v=+v_0$, where the interaction with the probe beam takes place, the time-dependent phase of both sublevel coherences is then given by $\exp[\pm i\omega_M t_0 \pm i\Omega_M(t-t_0)]$. In this second interaction zone the sublevel coherence together with the unmodulated probe field [$\sim \exp(i\omega_E t)$] produce, via a double-resonance process, coherent Raman fields oscillating at the sum and difference frequencies $\omega_E \pm \Omega_M$ [see Fig. 1(c)],

$$\exp(i\omega_E t)\exp[\pm i\omega_M t_0 \pm i\Omega_M(t-t_0)] \sim \exp[i(\omega_E \pm \Omega_M)t] . \quad (2.1)$$

In a steady-state experiment, the sublevel coherence is created at any time t_0. Thus, for a given velocity diffusion time $\tau=t-t_0$, the *steady-state* coherent Raman fields ($E_\pm$) oscillate at the frequencies $\omega_E \pm \omega_M$, as can be seen from (2.1) with the use of $\tau=t-t_0$,

$$E_\pm \sim \exp(i\omega_E t)\exp[\pm i\omega_M t_0 \pm i\Omega_M(t-t_0)] = \exp[i(\omega_E \pm \omega_M)t]\exp[\pm i(\Omega_M-\omega_M)\tau] . \quad (2.2)$$

The second factor in (2.2) reveals the phase shift occurring between the oscillating sublevel coherence (Ω_M) and the driving laser modulation (ω_M) during the velocity-diffusion process.

On a fast photodiode the Raman fields ($\omega_E \pm \omega_M$) together with the probe laser field (ω_E) yield a heterodyne beat signal of frequency $\omega_M = |\omega_E - (\omega_E \pm \omega_M)|$ [see Fig. 1(e)]. The amplitude and phase of this signal directly reveal the amplitude and phase of the sublevel coherence; thus, using a phase-sensitive detection scheme like a rf lock-in amplifier or a double balanced mixer, a phase-sensitive detection of the sublevel coherence is achieved.

The phase shift $(\omega_M-\Omega_M)\tau \equiv \Delta_M\tau$ resulting from the free evolution of the sublevel coherence in the field-free zone becomes especially noticeable in the output signal of the lock-in amplifier; as a consequence, a Ramsey-type interference pattern proportional to $\cos(\Delta_M\tau)$ appears in the signal line shape. This interference structure is observed by sweeping the sublevel detuning Δ_M and it becomes increasingly narrow for a larger diffusion time τ, i.e., for a larger distance between both interaction zones in velocity space. However, due to the distribution of diffusion times τ in the atomic ensemble, higher-order Ramsey fringes (large Δ_M) are essentially washed out.

In our experiment the motion of the active atoms in velocity space due to VCC plays a role similar to the spatial motion of the atoms in an atomic-beam Ramsey-resonance experiment. Quite analogously one expects to observe Ramsey fringes, if there is a separation between both interaction regions in velocity space, i.e., if the laser frequency Δ_E is detuned from the center of the Doppler profile.

A more detailed schematic of our experimental arrangement is shown in Fig. 2. The pump beam of frequency ω_E was phase modulated by means of an electro-optic modulation system (MS) to yield the modulation sidebands of frequency $\omega_E \pm \omega_M$. The carrier and sidebands were orthogonally polarized with respect to each other; the polarization direction of the carrier was chosen to be parallel to the transverse static magnetic field B that lifted the ground-state Zeeman-level degeneracy. In this way the carrier only drives the $m-m'=0$ (π) transition, whereas the sidebands solely couple the optical $m-m'=\pm 1$ (σ) transitions. This modulation and polarization scheme permits an excitation of Zeeman coherence in a single velocity subgroup only.

The counterpropagating probe beam was polarized parallel to the static magnetic field B and therefore only couples the optical π transition. The generated coherent Stokes and anti-Stokes Raman sidebands propagate in the same direction as the probe field. As a consequence of the selection rules, the Raman sidebands are linearly polarized in a direction that is perpendicular to the static magnetic field B. The total field behind the sample cell can be understood as a modulated laser field, which exhibits both an amplitude modulation (AM) and frequency modulation (FM) sideband structure.[16,17] These two modulation structures are related to different well-defined velocity-dependent detection sensitivities of Zeeman coherence;[18] it turns out that in our case the FM-sideband mode provides a resonant velocity-selective detection of the $\Delta m=1$ Zeeman coherence, as shown in Fig. 1(d). The FM sideband contributions can be monitored by means of a $\lambda/4$ plate which introduces an optical phase shift of $\pi/2$ between the carrier and the Raman sidebands.[18] The polarization analyzer A behind

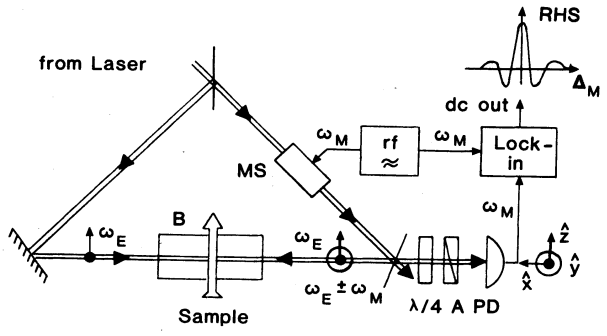

FIG. 2. Experimental scheme: MS, modulation system; B, static magnetic field; $\lambda/4$, retardation plate; A, polarization analyzer; PD, photodetector. The two principal axes of the $\lambda/4$ plate are oriented parallel to the $\hat{y}$ and $\hat{z}$ directions, respectively.

the $\lambda/4$ plate finally projects the carrier and Raman sidebands along a common direction in order to enable an optical interference at the photodiode (PD). The heterodyne beat signal is then detected by a phase-sensitive rf lock-in amplifier.

III. THEORY

In this section the Raman heterodyne signals (RHS) are calculated with the use of the density-matrix formalism, which describes the interaction of the atomic system with the laser fields. At first we solve the resulting equations of motion in the absence of collisions in order to explain the basic features of the velocity-selective excitation and detection of sublevel coherence. The effects of collisions of the active atoms with perturber atoms (buffer gas) are then taken into account and the modified equations of motion are solved in a perturbative treatment under steady-state conditions. The theoretical predictions on the influence of velocity-changing collisions are discussed and the resulting signal line shapes are interpreted as Ramsey-type resonances. Finally, explicit line-shape expressions are derived using a Fokker-Planck as well as a Keilson-Storer description of the velocity-diffusion process.

A. Atomic system and laser fields

Let us consider an atom consisting of a long-lived $J=1$ ground state and an optically excited state with angular momentum $J=0$, see Fig. 1(a). The ground-state m levels are split by a static magnetic field $\mathbf{B}$ applied in the $\hat{\mathbf{z}}$ direction which is chosen to be the quantization axis. A vapor of such four-level atoms interacts with a pump laser beam propagating perpendicular to the static magnetic field $\mathbf{B}$. The laser light is modulated at frequency ω_M; the corresponding spectral components are polarized in such a manner that the carrier with frequency ω_E only drives the π transition and that the sidebands with frequencies $\omega_\pm=\omega_E\pm\omega_M$ only couple the σ transitions,

$$\mathbf{E}_M=\left[\frac{E_\pi}{2}e^{i\omega_E t-ikx}+\text{c.c.}\right]\hat{\mathbf{z}}+\left[\frac{E_\sigma}{2}e^{i\omega_+ t-ik_+ x}+\text{c.c.}\right]\hat{\mathbf{y}}+\left[\frac{E_\sigma}{2}e^{i\omega_- t-ik_- x}+\text{c.c.}\right]\hat{\mathbf{y}}\ . \tag{3.1}$$

It should be mentioned here that a polarization scheme of this kind can experimentally be realized.

In addition to the modulated pump field, the vapor is irradiated either by a copropagating ($\epsilon=1$) or counterpropagating ($\epsilon=-1$) unmodulated probe beam with frequency ω_E,

$$\mathbf{E}_p=\left[\frac{E_p}{2}e^{i\omega_E t-i\epsilon kx}+\text{c.c.}\right]\hat{\mathbf{z}}\ . \tag{3.2}$$

The probe beam is linearly polarized and drives only the π transition.

The Hamiltonian for the atom is

$$H=H_0+H_I\ , \tag{3.3a}$$

$$H_I=-\boldsymbol{\mu}\cdot\mathbf{E}_M-\boldsymbol{\mu}\cdot\mathbf{E}_p\ , \tag{3.3b}$$

where H_0 is the free-atom Hamiltonian and H_I includes the atom-field interaction in the dipole approximation. In the basis of eigenstates $|i\rangle$ the relevant dipole matrix elements μ_{ij} are given by[18]

$$\mu_{24}=\mu_{42}=\langle 2\,|\,\boldsymbol{\mu}\cdot\hat{\mathbf{z}}\,|\,4\rangle\equiv\mu\ , \tag{3.4a}$$

$$\mu_{14}=\mu_{34}=\langle 1\,|\,\boldsymbol{\mu}\cdot\hat{\mathbf{y}}\,|\,4\rangle=-(i/\sqrt{2})\mu\ ; \tag{3.4b}$$

thus the nonvanishing matrix elements of the Hamiltonian can be written in the form

$$H_{44}=\hbar\Omega_E\ , \tag{3.5a}$$

$$H_{33}=-H_{11}=g_J\mu_B B\equiv\hbar\Omega_M\ , \tag{3.5b}$$

$$H_{24}=-\hbar(\alpha_\pi e^{i\omega_E t-ikx}+\text{c.c.})-\hbar(\alpha_p e^{i\omega_E t-i\epsilon kx}+\text{c.c.})\ , \tag{3.5c}$$

$$H_{14}=-i\hbar(\alpha_\sigma e^{i\omega_+ t-ik_+ x}+\text{c.c.})-i\hbar(\alpha_\sigma e^{i\omega_- t-ik_- x}+\text{c.c.})\ , \tag{3.5d}$$

$$H_{34}=H_{14}\ . \tag{3.5e}$$

Here g_J denotes the Landé g factor and μ_B is the Bohr magneton. The dipole coupling strengths α_π,α_σ, and α_p are defined by

$$\alpha_\pi=\frac{\mu E_\pi}{2\hbar}\ , \tag{3.6a}$$

$$\alpha_\sigma=-\frac{1}{\sqrt{2}}\cdot\frac{\mu E_\sigma}{2\hbar}\ , \tag{3.6b}$$

$$\alpha_p=\frac{\mu E_p}{2\hbar}\ . \tag{3.6c}$$

In Eqs. (3.6a)–(3.6c) α_π and α_p are taken to be real. In general, the coupling strength α_σ is complex; its phase reveals the modulation structure of the incident pump light, e.g., an imaginary α_σ describes a frequency modulation and a real α_σ an amplitude modulation of the pump beam, respectively.

B. Raman heterodyne signals in the absence of collisions

In this section we consider the excitation mechanism of optically induced sublevel coherence for atoms in a Doppler-broadened optical transition. It will be shown that individual multipole components can be created in a single velocity subgroup by a proper choice of the modulation structure of the excitation field. Further on we describe in detail the phase-sensitive detection of sublevel coherence with the use of the Raman heterodyne technique; finally, explicit line shapes are calculated for the case of a copropagating and a counterpropagating probe beam. At this stage, we will neglect the effects of collisions.

1. Velocity-selective excitation of sublevel coherence

We describe the behavior of the atomic system by means of the density-matrix formalism. The density-matrix equations of motion for an atomic ensemble with an axial velocity component v ($v=\mathbf{v}\cdot\hat{\mathbf{x}}$) are given by

$$\left[\frac{\partial}{\partial t}+v\frac{\partial}{\partial x}\right]\rho=-\frac{i}{\hbar}\left[H,\rho\right]+\cdots\ , \tag{3.7}$$

where the ellipses represent the phenomenological addition of damping terms. Although the Hamiltonian $H=H_0-\boldsymbol{\mu}\cdot\mathbf{E}_M-\boldsymbol{\mu}\cdot\mathbf{E}_p$ contains both the effects of the pump and probe fields ($\mathbf{E}_M$ and $\mathbf{E}_p$), we first consider only the interaction of the atoms with the pump beam. This simplification is valid for a sufficiently weak probe field, so that any pumping or relaxation effects due to the probe beam can be neglected; the interaction of the probe beam with the atomic ensemble will be treated later on in a lowest-order perturbation calculation.

The density-matrix equations (3.7) can be solved in a straightforward steady-state perturbation calculation (see Appendix A). With the assumption of equal dipole-coupling strengths ($|\alpha_\pi|=|\alpha_\sigma|$) and for the case of small sublevel detunings ($\Delta_M<\Gamma_E$), the relevant ground-state multipole components are given by

$$(-i\Delta_M+\gamma_{\rm tr})\tilde{\rho}_1^1(v)=\frac{i\alpha_\pi}{\sqrt{2}}(\alpha_\sigma^*-\alpha_\sigma)\tfrac{2}{3}NW(v)\frac{\Gamma_E}{(kv+kv_0)^2+\Gamma_E^2}\ , \tag{3.8a}$$

$$(-i\Delta_M+\gamma_{\rm tr})\tilde{\rho}_1^2(v)=\frac{i\alpha_\pi}{\sqrt{2}}(\alpha_\sigma^*+\alpha_\sigma)\tfrac{2}{3}NW(v)\frac{\Gamma_E}{(kv+kv_0)^2+\Gamma_E^2}\ . \tag{3.8b}$$

Here, we have written the transverse orientation $\tilde{\rho}_1^1$ and the transverse alignment $\tilde{\rho}_1^2$ in the field-interaction representation

$$\rho_1^1=\tilde{\rho}_1^1 e^{-i\omega_M t}\ , \tag{3.9a}$$

$$\rho_1^2=\tilde{\rho}_1^2 e^{-i\omega_M t}\ . \tag{3.9b}$$

In Eqs. (3.8a) and (3.8b), N is the atomic-number density and $W(v)$ denotes the one-dimensional Maxwell-Boltzmann velocity distribution [see Eq. (A8b) in Appendix A] with u being the most probable speed in thermal equilibrium. The Doppler width given by ku, is assumed to be large compared to the homogeneous optical linewidth Γ_E that is determined by the spontaneous decay of the optically excited state. The rate $\gamma_{\rm tr}$ phenomenologically describes the decay of the multipole components towards thermal equilibrium due to the transit time of the atoms through the laser beam. The detuning parameters are defined by

$$\Delta_M=\omega_M-\Omega_M\ , \tag{3.10a}$$

$$kv_0=\Delta_E=\Omega_E-\omega_E\ , \tag{3.10b}$$

where v_0 is the velocity of those atoms that are resonantly driven by the laser field.

The result (3.8a) and (3.8b) describes the velocity-selective creation of oscillating ground-state sublevel coherence caused by modulated, narrow bandwidth laser excitation of a Doppler-broadened optical transition. If the modulation structure of the driving pump field is chosen properly, *individual* multipole components can be induced; an amplitude-modulated pump field (α_σ is real) results in an excitation of transverse alignment, whereas a frequency-modulated field (α_σ is imaginary) only creates a transverse orientation.

If the modulation frequency ω_M is tuned, a narrow resonance is created for $\Delta_M=\omega_M-\Omega_M=0$. The width of this resonance is solely determined by the effective lifetime $1/\gamma_{\rm tr}$ of the ground-state sublevel coherence and can thus be much narrower than the optical linewidth Γ_E. Furthermore, the width of the sublevel resonance is not affected by laser frequency jitter, since only the frequency difference of the carrier and sidebands of the driving laser field is essential for the occurrence of the resonance.

2. Signal detection

A phase-sensitive detection of sublevel coherence is attainable by means of the Raman heterodyne technique. In Appendix B we derive expressions for the Raman heterodyne signals related to the special case considered in this paper; here, we only present the calculated results.

In the following we suppose that the sublevel coherence has been excited by a *frequency modulated* pump beam. It is shown in Appendix B that in this case only the Raman heterodyne signals obtained in the FM-detection mode permit a velocity-selective detection of sublevel coherence. The resulting "in-phase" and "quadrature" Raman heterodyne signals ($S_{\rm in}$ and $S_{\rm qu}$) can be written as

$$S_{\rm in}=E_p^2\,{\rm Re}(m_{\rm FM})\ , \tag{3.11a}$$

$$S_{qu}=E_p^2\,{\rm Im}(m_{\rm FM})\ , \tag{3.11b}$$

where the modulation parameter $m_{\rm FM}$ is given by

$$m_{\rm FM}=\frac{kL}{\epsilon_0}\mu\frac{\alpha_p}{2E_p}\int_{-\infty}^{+\infty}dv\,\tilde{\rho}_1^1(v)\frac{\Gamma_E}{(kv_0+\epsilon kv)^2+\Gamma_E^2}\ . \tag{3.12}$$

This result allows the calculation of the RHS providing the velocity distribution of the transverse orientation $\tilde{\rho}_1^1(v)$ is known. The resonance denominator in Eq. (3.12) illustrates the velocity-selective detection sensitivity for $\tilde{\rho}_1^1(v)$; the main contributions to the RHS stem from those atoms with velocities $v=-\epsilon v_0$.

In the absence of collisions, explicit RHS line shapes can be obtained with the use of the perturbation solution for $\tilde{\rho}_1^1(v)$, Eq. (3.8a). In the Doppler limit ($ku\gg\Gamma_E$) the following in-phase and quadrature signals are derived:

$$S_{\rm in}\sim E_p\mu\alpha_p\alpha_\pi|\alpha_\sigma|\frac{\gamma_{\rm tr}}{\Delta_M^2+\gamma_{\rm tr}^2}\frac{\Gamma_E}{[(kv_0-\epsilon kv_0)/2]^2+\Gamma_E^2}\times e^{-(v_0/u)^2}\ , \tag{3.13a}$$

$$S_{\rm qu} \sim E_p \mu \alpha_p \alpha_\pi \mid \alpha_\sigma \mid \frac{\Delta_M}{\Delta_M^2+\gamma_{\rm tr}^2} \frac{\Gamma_E}{[(kv_0-\epsilon kv_0)/2]^2+\Gamma_E^2} \times e^{-(v_0/u)^2} . \quad (3.13b)$$

The signal dependence on the laser frequency detuning $\Delta_E = kv_0$ recovers for a copropagating probe beam ($\epsilon=1$) the Doppler profile $\exp[-(v_0/u)^2]$, whereas for a counterpropagating probe ($\epsilon=-1$) a Doppler-free Lorentzian resonance of width Γ_E centered at $kv_0=0$ is obtained. As a function of the sublevel detuning Δ_M the signals show in both cases ($\epsilon=\pm 1$) Lorentzian resonances of width $\gamma_{\rm tr}$ reflecting the resonance behavior of the sublevel coherence.

3. *Relationship to four-wave-mixing processes*

In terms of nonlinear optics, the Raman heterodyne technique discussed here can also be interpreted as a resonant four-wave-mixing process.[19] This is reflected in Eqs. (3.13) by the threefold product of dipole-coupling strengths ($\alpha_p \alpha_\pi \mid \alpha_\sigma \mid$) thus indicating a third-order process. The three ingoing waves forming part of the nonlinear wave-mixing process consist of one of the sideband fields with frequency $\omega_E \pm \omega_M$, the carrier field (ω_E), and the probe field (ω_E). For simplicity we will restrict the following discussion to the presence of only the upper sideband with frequency $\omega_E+\omega_M$; it will become clear that similar considerations also hold for the lower-sideband case.

The corresponding four-wave-mixing process can then be depicted schematically as shown in Fig. 3(a); the modulation sideband (E_σ) and the carrier field (E_π) drive the sublevel coherence via a resonance Raman transition; the probe field (E_p) resonantly couples to this sublevel coherence and yields the coherent Raman sideband at frequency $\omega_E+\omega_M-\omega_E+\omega_E=\omega_E+\omega_M$. Let us assume that the pump and the probe beam propagate under some angle θ with $0 \le \theta \le 180°$ [see Fig. 3(b)]. With $\mathbf{k}_p$ denoting the wave vector of the probe beam, the phase-matching condition then reads $\mathbf{k}_+ - \mathbf{k} + \mathbf{k}_p \simeq \mathbf{k}_p$, i.e., phase matching is fulfilled automatically for modulation frequencies ω_M in the rf and microwave range $[(\omega_M/\omega_E) \ll 1]$. As a consequence, the fourth wave is emitted always in the same direction as the ingoing probe field and thus can be detected easily via optical heterodyning on a fast photodetector with the probe field acting as a local oscillator. Obviously, this wave-mixing process can also be viewed as a multiresonant coherent anti-Stokes Raman scattering (CARS) process.[19]

As already discussed above, in principle two different geometries are possible corresponding to copropagating ($\epsilon=+1$, $\theta=0$) and counterpropagating ($\epsilon=-1$, $\theta=180°$) pump and probe fields, respectively. (i) $\epsilon=+1$: In practice, the pump and probe fields will be sent into the sample under some small angle $\theta \ll 1$; otherwise the probe beam signal cannot be detected separately. This situation was realized experimentally in studies of Zeeman coherence in the sodium ground state using the Raman heterodyne technique.[4] (ii) $\epsilon=-1$: With no collisions being present, a Doppler-free signal occurs for $\Delta_E=0$ when the Doppler detuning Δ_E is varied for a fixed modulation frequency ω_M. If at the same time the sublevel detuning $\Delta_M=\omega_M-\Omega_M$ equals zero, the Doppler-free heterodyne signal displays a resonance Raman enhancement; this phenomenon was observed recently in Sm vapor on the Sm $\lambda=570.68$-nm line.[20]

The geometry of counterpropagating pump and probe fields is of special interest with respect to the present work; in the following we will analyze the occurrence of Raman heterodyne signals for a *nonzero* Doppler detuning. It will become obvious that new signal features arise in the presence of velocity-changing collisions.

C. Raman heterodyne signals in the presence of collisions

When buffer-gas atoms are present in the sample cell, collisional relaxation and redistribution of the density-matrix elements have to be considered. In our treatment we regard the effects of both depolarizing and velocity-changing collisions on the ground-state sublevel coherence of the atoms. In contrast to this, we neglect the effects of VCC on the optical coherences and only take into account the collisional dephasing of the optical dipoles. With these assumptions, the corresponding density-matrix equations of motion can be solved in a steady-state perturbation calculation which yields the velocity distribution of sublevel coherence. In this section we calculate the resulting RHS supposing a frequency-

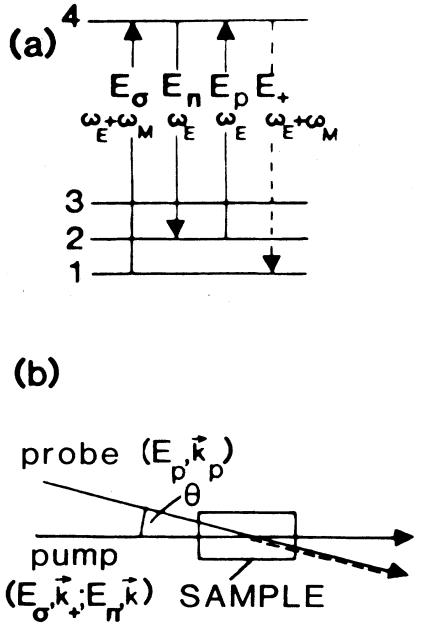

FIG. 3. (a) Diagram for the representation of the Raman-resonant four-wave-mixing process. The created Raman sideband is depicted by the dashed line. (b) Schematic of the beam geometry. Pump and probe field propagate under some angle θ with respect to each other. $\mathbf{k}_+$ and $\mathbf{k}$ are the wave vectors of the pump field components E_σ and E_π, respectively; $\mathbf{k}_p$ denotes the wave vector of the probe field E_p.

modulated pump and a counterpropagating probe beam. It will be shown that the resonance structure of the monitored sublevel coherence reveals the temporal behavior of the velocity-diffusion process caused by collisions; the obtained signal line shapes show the characteristics of the well-known Ramsey fringes.

1. *Velocity distribution of sublevel coherence*

In order to describe the influence of the collisional relaxation and redistribution effects on the density matrix, one can simply add to the equations of motion (3.7) appropriate damping and transport terms arising from collisions.[8]

The collisional dephasing of the optical dipoles leads to a pressure broadening $\Gamma_{\rm col}$ of the homogeneous optical linewidth Γ_E; thus we simply replace Γ_E by $\Gamma = \Gamma_E + \Gamma_{\rm col}$. The sublevel multipole components are assumed to decay isotropically, i.e., we ignore possible collisional coupling between different multipoles. The relaxation rate for the considered transverse orientation may be written as $\gamma = \gamma_{\rm tr} + \gamma_{\rm col}$ where $\gamma_{\rm tr}$ describes the effects of a finite transit time in the laser beam and $\gamma_{\rm col}$ denotes the depolarizing collision rate. The collisional transfer of the orientation with axial velocity v' to other velocities v is described by the real collision kernel $W(v' \to v)$; the corresponding rate for VCC is given by

$$\gamma_{\rm VCC} = \int dv' W(v' \to v) \ . \tag{3.14}$$

For simplicity, all rate constants are taken to be velocity independent. Under these assumptions one obtains the following transport equation for the transverse orientation $\tilde{\rho}_1^1(v)$:

$$(-i\Delta_M + \gamma + \gamma_{\rm VCC})\tilde{\rho}_1^1(v) = I(v) + \int dv' W(v' \to v)\tilde{\rho}_1^1(v') \ , \tag{3.15}$$

where $I(v)$ reveals the velocity selectivity of the laser excitation,

$$I(v) = \alpha_\pi \, | \, \alpha_\sigma \, | \, \frac{2}{3}\frac{1}{\sqrt{2}} N W(v) \frac{\Gamma}{(kv_0 + kv)^2 + \Gamma^2} \ . \tag{3.16}$$

The formal solution of (3.15) is given by[21]

$$\tilde{\rho}_1^1(v) = \int dv' G(v' \to v) I(v') \ , \tag{3.17}$$

where the propagator $G(v' \to v)$ satisfies the propagator equation

$$(-i\Delta_M + \gamma + \gamma_{\rm VCC}) G(v' \to v) = \delta(v - v') + \int dv'' G(v' \to v'') W(v'' \to v) \ . \tag{3.18}$$

Instead of solving (3.18) directly, we write $G(v' \to v)$ in the form

$$G(v' \to v) = \int_0^\infty dt \, p(v' \to v, t) e^{-(\gamma - i\Delta_M)t} \ , \tag{3.19}$$

where $p(v' \to v, t)$ is the solution of the Boltzmann transport equation,

$$\frac{\partial}{\partial t} p(v' \to v, t) = -\gamma_{\rm VCC} p(v' \to v, t) + \int dv'' p(v' \to v'') W(v'' \to v) \ , \tag{3.20}$$

with the initial condition $p(v' \to v, t=0) = \delta(v - v')$. The Laplace transformation (3.19) provides a simple interpretation of the RHS line shape as will become obvious later on. The function $p(v' \to v, t)$ denotes the probability to find an atom at time t with velocity v, if it had a velocity v' at time $t = 0$. The velocity distribution of $\tilde{\rho}_1^1(v)$ can then be written as

$$\tilde{\rho}_1^1(v) = \int_0^\infty dt \int_{-\infty}^{+\infty} dv' I(v') p(v' \to v, t) e^{-(\gamma - i\Delta_M)t} \ . \tag{3.21}$$

This result can be simplified, if we consider the velocity distribution of $\tilde{\rho}_1^1(v)$ only for velocities v lying far outside the initially excited subgroup, $| v + v_0 | \gg \Gamma/k$. In this case $I(v')$ in the integrand is a highly peaked function around $v' = -v_0$; the integration over v' can then be performed and one obtains

$$\tilde{\rho}_1^1(v) = \frac{2}{3}\left[\frac{\pi}{2}\right]^{1/2} \alpha_\pi \, | \, \alpha_\sigma \, | \, \frac{N}{ku} e^{-(v_0/u)^2} \times \int_0^\infty dt \, p(-v_0 \to v, t) e^{-(\gamma - i\Delta_M)t} \ . \tag{3.22}$$

This equation describes the collisional velocity distribution of the sublevel coherence $\tilde{\rho}_1^1$. The time t itself can be interpreted as the time that has passed since the excitation of the sublevel coherence. A group of atoms that needs a time t for the diffusion process from $-v_0$ to v yields a contribution to $\tilde{\rho}_1^1(v)$ that is proportional to $\exp[(-\gamma + i\Delta_M)t]$. The factor $\exp(-\gamma t + i\Delta_M t)$ characterizing a single contribution can then be understood as follows: the first exponential just reflects the decay of sublevel coherence during the diffusion time t; the second term gives rise to an accumulating phase shift $\Delta_M t$ between the oscillating sublevel coherence and the driving modulation of frequency ω_M. The coherence $\tilde{\rho}_1^1$ is thus seen to oscillate during the velocity-diffusion process at its eigenfrequency $\Omega_M = \omega_M - \Delta_M$. This behavior may be interpreted as a free evolution of the sublevel coherence in time; if the active atoms have been removed from the optically excited velocity subgroup, no interaction between the atoms and the laser fields takes place due to the Doppler effect. The integration in (3.22) can be interpreted as a weighted average of the sublevel coherence contributions over all possible times t.

2. *Signal line shapes: Interpretation as Ramsey resonances*

We can now calculate the Raman heterodyne signals referring to the results of Sec. III B. In the FM-detection mode the counterpropagating probe beam picks up the sublevel coherence in the velocity subgroup $v = v_0 \pm \Gamma/k$. In the Doppler limit we obtain for the modulation parameter $m_{\rm FM}$, by use of Eq. (3.12) and (3.22),

$$m_{\mathrm{FM}}=(C_{\mathrm{FM}}/E_p^2)e^{-(v_0/u)^2} \times \int_0^\infty dt\, p(-v_0\rightarrow v_0,t)e^{-(\gamma-i\Delta_M)t} , \quad (3.23)$$

where

$$C_{\mathrm{FM}}=\frac{1}{3}N\frac{\pi^{3/2}kL}{\sqrt{2}\epsilon_0}\frac{\mu E_p\alpha_p\alpha_\pi|\alpha_\sigma|}{k^2u} . \quad (3.24)$$

The resulting in-phase and quadrature RHS are then given by

$$S_{\mathrm{in}}=\int_0^\infty dt\, F(t)\cos(\Delta_M t) , \quad (3.25a)$$

$$S_{\mathrm{qu}}=\int_0^\infty dt\, F(t)\sin(\Delta_M t) , \quad (3.25b)$$

where

$$F(t)=C_{\mathrm{FM}}e^{-(v_0/u)^2}p(-v_0\rightarrow v_0,t)e^{-\gamma t} . \quad (3.26)$$

Let us now discuss some properties of the signal line shapes (3.25a) and (3.25b) without an explicit use of a particular velocity distribution $p(-v_0\rightarrow v_0,t)$. The signals depend on two detuning parameters, the laser frequency detuning $\Delta_E=kv_0$ within the Doppler profile and the detuning Δ_M of the modulation frequency ω_M from the Zeeman splitting Ω_M. The corresponding signal line shapes have a simple interpretation, when we consider the signal dependence on the sublevel detuning for a fixed laser frequency detuning $\Delta_E\neq 0$; the signal equations (3.25a) and (3.25b) have the same form as those equations derived for the description of usual Ramsey-resonance experiments in atomic beams, where the atoms pass two rf fields separated in local space.[22] In our case, the atoms move in velocity space from the velocity $-v_0$ to $+v_0$ due to VCC. During the time required for the velocity-diffusion process no interaction between the atoms and the laser fields takes place and the sublevel coherence thus evolves at its eigenfrequency Ω_M. The corresponding phase shift $\Delta_M t$ between the oscillating coherence and the driving modulation results in a signal contribution that is proportional to $\cos(\Delta_M t)$, thereby showing the well-known Ramsey fringe pattern. In order to obtain the entire signal, one has to average the signal contributions over the distribution of diffusion times $F(t)$.

A qualitative plot of the function $F(t)$ is shown in Fig. 4. For an increasing time t, $p(-v_0\rightarrow v_0,t)$ typically increases towards the thermalization value given by the Boltzmann velocity distribution. If the decay factor $\exp(-\gamma t)$ is taken into account, $F(t)$ displays a certain maximum at time $t=\tau$. Thus the main contribution to the signal stems from atoms with sublevel coherence with this most probable diffusion time τ and one expects to see Ramsey fringes proportional to $\cos(\Delta_M\tau)$. Of course, to a certain degree the fringe structure is washed out due to the width of the distribution function $F(t)$. The value of the most probable diffusion time τ as well as the width of the distribution function $F(t)$ are partly determined by the decay term $\exp(-\gamma t)$; it turns out that the decay of sublevel coherence is essential for the occurrence of the Ramsey fringes. This is in contrast to the behavior of Ramsey resonances obtained in atomic-beam experiments, where a decay term results in a decrease of the resonance amplitude rather than in a change of the fringe pattern. Quantitative RHS line shapes can only be obtained by choosing a specific collision model that gives rise to a corresponding distribution function $p(-v_0\rightarrow v_0,t)$.

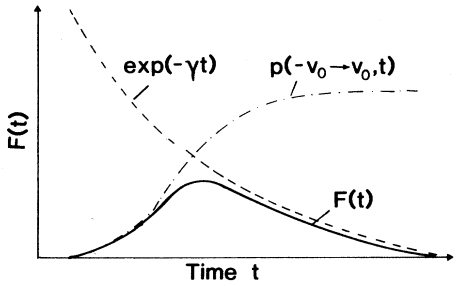

FIG. 4. Outline of the distribution function $F(t)$ (solid line: ——) for the velocity-diffusion process from velocity $-v_0$ to $+v_0$. $F(t)$ is decomposed into a product of two functions: $p(-v_0\rightarrow v_0,t)$ describes the collisional velocity diffusion of the active atoms with sublevel coherence neglecting loss terms, whereas the exponential $\exp(-\gamma t)$ describes the losses of sublevel coherence.

Just as in the absence of collisions, the signal formation can be interpreted again as a four-wave-mixing process. In the presence of collisions and for a nonzero laser detuning Δ_E, however, a certain time delay between the coherent excitation and detection processes is present due to the finite diffusion time τ; the four-wave-mixing process is "split" into two parts which occur successively with the time delay τ.

3. *Fokker-Planck model*

The calculation of the Raman heterodyne signals requires a solution of the Boltzmann transport equation (3.20) with the use of a particular collision kernel $W(v'\rightarrow v)$. However, the basic features of the line shapes can be explained with a much simpler approach: if we assume a Brownian-motion-type collision model, i.e., "weak" collisions, and if we consider times that are large compared to the inverse collision rate ($t\gamma_{\mathrm{VCC}}\gg 1$), the Boltzmann equation reduces to a Fokker-Planck (FP) equation.[15,23]

The first condition can be adopted if the mass ratio of the perturber and active atoms is much less than unity ($m_p/m_A\ll 1$); the second condition can be met, if significant signal contributions only arise for times $t\gg 1/\gamma_{\mathrm{VCC}}$, i.e., if it takes several collisions for a transfer from the velocity $-v_0$ to $+v_0$. This condition demands a laser frequency detuning kv that is larger than the Doppler shift $k\Delta u$ ($kv_0\gg k\Delta u$) resulting from the characteristic collisional velocity change Δu and that is larger than the bandwidth Γ ($kv_0\gg\Gamma$) of the initially prepared atomic subgroup.

The solution of the resulting Fokker-Planck equation

$$\frac{\partial}{\partial t}p(v_0\rightarrow v,t) = \gamma_{\rm th}\frac{\partial}{\partial v}[vp(v_0\rightarrow v,t)]+\gamma_{\rm th}\frac{u^2}{2}\frac{\partial^2}{\partial v^2}p(v_0\rightarrow v,t)\ , \tag{3.27}$$

with the initial condition $p(v_0\rightarrow v,t=0)=\delta(v-v_0)$. $p(v_0\rightarrow v,t)$ is given by[15,24]

$$p(v_0\rightarrow v,t) = \frac{1}{\sqrt{\pi}u\,[1-\exp(-2\gamma_{\rm th}t)]^{1/2}} \times\exp\left[-\frac{[v-v_0\exp(-\gamma_{\rm th}t)]^2}{u^2[1-\exp(-2\gamma_{\rm th}t)]}\right]. \tag{3.28}$$

The solution (3.28) describes at any time a Gaussian velocity distribution of width $u\,[1-\exp(-2\gamma_{\rm th}t)]^{1/2}$ centered at $v_0\exp(-\gamma_{\rm th}t)$. The rate $\gamma_{\rm th}$ can be interpreted as an effective decay rate of a given velocity anisotropy towards thermal equilibrium; it is related to the collision rate $\gamma_{\rm VCC}$ and to the collisional velocity change Δu by[15]

$$\gamma_{\rm th}=\gamma_{\rm VCC}\frac{1}{2}\left[\frac{\Delta u}{u}\right]^2. \tag{3.29}$$

With the use of the solution (3.28) the in-phase RHS is obtained according to Eq. (3.25a) with $F(t)$ given by

$$F(t)=\frac{C_{\rm FM}\exp[-(v_0/u)^2]}{\sqrt{\pi}u[1-\exp(-2\gamma_{\rm th}t)]^{1/2}} \times\exp\left[-\gamma t-\left[\frac{v_0}{u}\right]^2\frac{1+\exp(-\gamma_{\rm th}t)}{1-\exp(-\gamma_{\rm th}t)}\right]. \tag{3.30}$$

For a given laser frequency detuning the signal line shape thus depends on two parameters only, the thermalization rate $\gamma_{\rm th}$ and the decay rate γ of the sublevel coherence. However, the characteristic form of the sublevel resonance is solely determined by the ratio $\gamma_{\rm th}/\gamma$, which describes the degree of collisional thermalization within the lifetime of the sublevel coherence.

A simple analytical line-shape expression can only be obtained in the limit $\gamma_{\rm th}/\gamma\rightarrow\infty$, i.e., in the limit of an infinite ground-state lifetime. Then a complete thermalization of the sublevel coherence velocity distribution takes place and Eq. (3.25a) yields

$$S_{\rm in}(\Delta_M)\rightarrow\frac{C_{\rm FM}\exp[-(v_0/u)^2]}{\sqrt{\pi}u}\frac{\gamma}{\Delta_M^2+\gamma^2}\ . \tag{3.31}$$

In this limit, as well as in the absence of collisions ($\gamma_{\rm VCC}/\gamma=0$, see Sec. III B 2), the RHS show Lorentzian resonances of width γ; no Ramsey resonance structure is obtained.

For other values of $\gamma_{\rm th}/\gamma$, the integration has to be performed numerically. A typical result of a numerical line-shape calculation according to Eqs. (3.25a) and (3.30) is shown in Fig. 5, where the in-phase RHS are displayed as a function of the sublevel detuning Δ_M for different laser frequency detunings kv_0. It can be seen that the line shape of the resonances drastically depends on the laser detuning; especially for large detunings kv_0 the Ramsey resonance pattern becomes more and more pronounced. This is in contrast to the behavior of Ramsey resonances observed in atomic-beam experiments, where a larger distance between both interaction zones only leads to a reduction of the resonance linewidth and not to a change of the Ramsey fringe pattern.

Figure 5 also shows that the linewidth of the sublevel resonances decreases with increasing laser detuning kv and can yield values that lie below the "natural" limit that is given by the lifetime $1/\gamma$ of the sublevel coherence. This linewidth narrowing is a direct consequence of the collisional diffusion process in velocity space: the typical time required for the diffusion of atoms with sublevel coherence from velocity $-v_0$ to $+v_0$ becomes larger for a larger "distance" in velocity space; hence, only the fraction of atoms whose sublevel coherence has "survived" during the period of the diffusion process can contribute to the signal. If this period is larger than the lifetime $1/\gamma$ of the sublevel coherence, the corresponding signal contribution shows resonance structures that are narrower than expected from the lifetime $1/\gamma$.

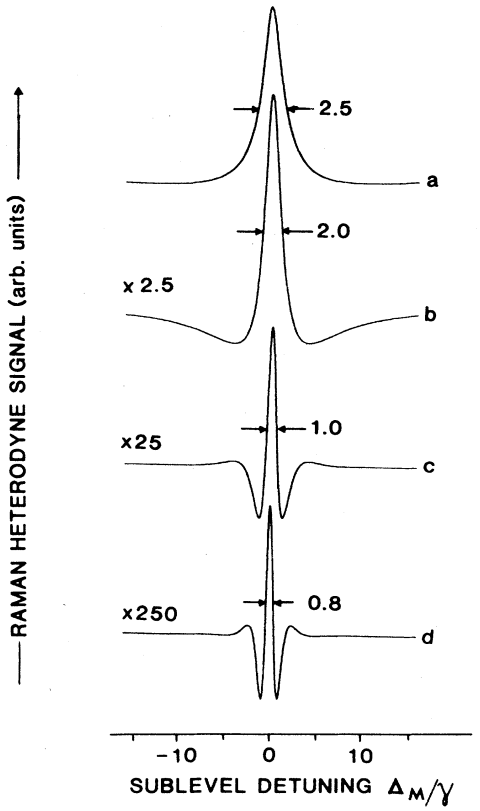

FIG. 5. Calculated RHS as a function of the normalized sublevel detuning Δ_M/γ for different normalized laser frequency detunings $\Delta_E/\sigma_E=v_0/u$: (a, $v_0/u=0.10$; b, $v_0/u=0.19$; c, $v_0/u=0.57$; d, $v_0/u=0.86$). The calculation is based on the FP description using the parameter value $\gamma_{\rm th}/\gamma=0.18$. The resulting RHS show narrow interference patterns of widths lying below the value 2γ; a linewidth (FWHM) of 2γ corresponds to the lifetime $1/\gamma$ of the sublevel coherence.

As a measure for this "typical" time t one may regard the most probable diffusion time τ; in the case $\gamma_{\rm th}/\gamma \ll 1$ (incomplete thermalization) we obtain approximately a linear relationship between τ and v_0/u,

$$\tau \simeq \left[\frac{2}{\gamma_{\rm th}\gamma}\right]^{1/2}\left|\frac{v_0}{u}\right| . \tag{3.32}$$

Consequently, the width of the sublevel resonance is expected to be roughly proportional to the inverse laser frequency detuning within the Doppler profile.

Figure 5 also indicates that the RHS amplitudes strongly decrease with increasing laser detuning. One may again derive a simple expression for the RHS amplitude in the limit $\gamma_{\rm th}/\gamma \ll 1$,

$$S_{\rm in}(\Delta_M=0) = \frac{C_{\rm FM}}{u}\left[\frac{1}{2\gamma_{\rm th}\gamma}\right]^{1/2} \times \exp\left[-\left[\frac{v_0}{u}\right]^2 - 2\left[\frac{2\gamma}{\gamma_{\rm th}}\right]^{1/2}\left|\frac{v_0}{u}\right|\right] . \tag{3.33}$$

This line shape is the usual Gaussian Doppler profile multiplied by a narrow exponential that may be written in the form

$$\exp\left[-2\left[\frac{2\gamma}{\gamma_{\rm th}}\right]^{1/2}\left|\frac{v_0}{u}\right|\right] = \exp(-2\gamma\tau) , \tag{3.34}$$

where we have used the expression (3.32) for the most probable diffusion time τ. This result indicates that the decrease of the RHS amplitude mainly stems from the decay of sublevel coherence during the time required for the diffusion process.

4. *Keilson-Storer model*

If the assumptions made in the Fokker-Planck approximation cannot be justified, one has to seek for a solution of the more general Boltzmann integral equation (3.20) with the use of a specific collision kernel $W(v'\to v)$. Here we choose the phenomenological and analytically tractable Keilson-Storer (KS) kernel[23]

$$W(v'\to v) = \frac{\gamma_{\rm VCC}}{\sqrt{\pi}\Delta u}\exp\left[-\left[\frac{v-\alpha v'}{\Delta u}\right]^2\right] , \tag{3.35}$$

where $\Delta u = u(1-\alpha^2)^{1/2}$ is the kernel width. The parameter α $(0\le\alpha<1)$ describes the strength of the collisions; if, e.g., α is close to one, the collisions are weak, whereas for $\alpha=0$ one collision is sufficient to thermalize the sample. The solution of the Boltzmann equation (3.20) with the kernel (3.35) is given by[23]

$$p(v'\to v,t) = e^{-\gamma_{\rm VCC}t}\left[\delta(v'-v) + \sum_{n=1}^{\infty}\frac{(\gamma_{\rm VCC}t)^n}{n!}W_n(v'\to v)\right] , \tag{3.36a}$$

with

$$W_n(v'\to v) = \frac{1}{\sqrt{\pi}\Delta u_n}\exp\left[-\left[\frac{v-\alpha^n v'}{\Delta u_n}\right]^2\right] , \tag{3.36b}$$

$$\Delta u_n = u(1-\alpha^{2n})^{1/2} . \tag{3.36c}$$

Using this solution we find according to Eqs. (3.25a) and (3.26) for the in-phase RHS in the limit $kv_0 \gg \Gamma$

$$S_{\rm in} = \frac{C_{\rm FM}e^{-(v_0/u)^2}}{\gamma_{\rm VCC}} \times \sum_{n=1}^{\infty}\left[\frac{\gamma_{\rm VCC}^2}{\Delta_M^2+(\gamma+\gamma_{\rm VCC})^2}\right]^{(n+1)/2} \times W_n(-v_0\to v_0)\cos[(n+1)\phi] \tag{3.37a}$$

with

$$\tan\phi = \Delta_M/(\gamma+\gamma_{\rm VCC}) . \tag{3.37b}$$

Line shapes analogous to (3.37) have been derived from the analysis of optical-pumping experiments with the direction of the pumping polarization being modulated.[11] In (3.37), the nth summand describes the average effect of n collisions; the corresponding sublevel resonance displays a fringe structure proportional to $\cos[(n+1)\phi]$ that becomes increasingly narrow for large n, i.e., for a large diffusion time $t \approx n/\gamma_{\rm VCC}$. The entire signal is obtained by summing up the contributions arising from all collision events; as a consequence, the fringe pattern will again be washed out to a certain extent.

The parameters α, $\gamma_{\rm VCC}$, and γ can in principle be determined by fitting the line shape (3.37) to the measured curves. In Sec. V we describe the results of such fitting attempts based on both the KS and the FP model.

IV. EXPERIMENT

The experiments were performed in atomic samarium vapor using the Sm $\lambda=570.68$-nm $4f^6 6s^2\,{}^7F_1 \to 4f^6 6s 6p\,{}^7F_0$ line for optical excitation. In this particular Sm transition it is possible to excite a single even $(I=0)$ Sm isotope component; thus an essentially pure $J=1-J'=0$ transition is experimentally accessible. The collision studies were carried out with rare-gas perturbers at various pressures; due to the low Sm number density used in the experiments (see Sec. IV A 2), collisions between Sm atoms were neglible.

In this section we will first give some details of the experimental apparatus and then present the main results of the measurements.

A. Experimental arrangement

The experimental setup is shown schematically in Fig. 2. The beam of a single-mode cw dye ring laser (bandwidth 10 MHz) was split into two parts in order to yield the counterpropagating pump and probe beams, which were then spatially superimposed in the Sm vapor cell. The laser-beam diameters ($1/e$ intensity drop) of the pump and probe beams in front of the sample cell were

0.8 and 0.5 mm, respectively. The optical power typically was about 1.5 mW in each beam. At these laser intensities the observed Raman heterodyne signals did not show any saturation behavior.

1. The modulation system

The pump beam was modulated at the rf frequency $\omega_M = 2\pi \times 10.0$ MHz to produce the optical sideband fields with frequencies $\omega_E \pm \omega_M$; the corresponding electro-optic modulation system is depicted in Fig. 6. The ingoing pump beam was linearly polarized in a direction parallel to the static magnetic field **B** and then sent through a transverse electro-optic modulator (Gsänger LM 202). The modulator consists of two pairs of orthogonally arranged ammonium dihydrogen phosphate (ADP) crystals to compensate for temperature drifts of the birefringence. The main axes of the ADP crystals were oriented at 45° with respect to the polarization direction of the incident laser beam. This configuration permits a modulation scheme of the laser light, where the modulation sidebands are polarized perpendicular to the external field **B**, while the carrier is polarized parallel to the B field; in addition, the carrier and sideband fields exhibit a phase relationship corresponding to a pure frequency modulation.[25] Although carrier and sidebands have orthogonal polarization directions, the laser beam can be regarded in a more general sense as being frequency modulated.

The modulator was part of a resonantly tuned LC circuit driven by a frequency synthesizer (Rhode und Schwartz SMS) in combination with a rf power amplifier (ENI 310L). With an applied rf power of 0.1 W the produced laser sidebands contained about 3% of the incident laser power. Thus the corresponding modulation depth was low enough to neglect signal effects due to the generation of higher-order sidebands at frequencies $\omega_E \pm n\omega_M$ $(n > 1)$. On the other hand, due to this low modulation depth the amplitude of the carrier E_π was much larger than the sideband amplitude E_σ. In order to meet the theoretical requirement of equal dipole coupling strengths for the π and σ transitions of the Sm line, we attenuated the carrier with respect to the sidebands by using the polarization dependence of the reflection coefficient of an uncoated quartz plate oriented near Brewster's angle. The fine tuning of the required amplitude ratio $E_\pi/E_\sigma = 1/\sqrt{2}$ was achieved by controlling the modulation depth via the rf input power. Finally, a second electro-optic device (EOD PC19) was used to compensate for possible phase shifts between the carrier and sideband fields resulting from reflections at the dielectrically coated mirrors.

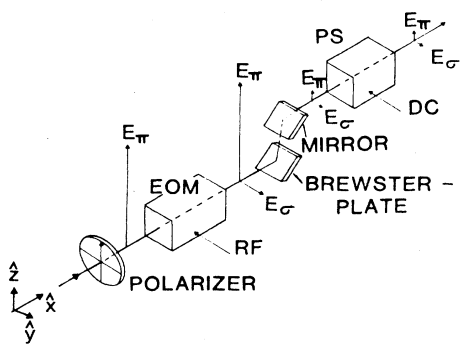

FIG. 6. Outline of the modulation system to yield orthogonally polarized carrier (E_π) and sideband (E_σ) fields of adjustable strengths and definite phase relationship. EOM, electro-optic modulator; PS, electro-optic phase shifter (for details see text).

The proper alignment of the whole modulation system was controlled by monitoring the beat signal of carrier and sidebands after their passing through an analyzer to allow for interference. In the case of a pure frequency-modulated light beam the beat signal should not show any intensity modulation at the modulation frequency ω_M. In practice, however, the light beam contained spurious AM contributions; the amount of the residual AM-sideband amplitude was measured to be less than 1.5% compared to the corresponding FM-sideband amplitude.

2. The sample

Natural Sm consists of seven isotopes; among these isotopes ^{152}Sm and ^{154}Sm are the most abundant ones.[26] The considered $\lambda = 570.68$-nm Sm line possesses large isotope shifts with the ^{154}Sm line lying at the end of the low-frequency side and the next isotope component being the ^{152}Sm line with a $+990$-MHz separation.[27] According to the Landé factor of $g_J = 1.5$ for the $J = 1$ ground state of the even Sm isotopes,[28] the Bohr frequency of the Zeeman splitting between the m sublevels is given by $\Omega_M = 2\pi \times 21.0$ MHz (B/mT). Using cell temperatures of about 1000 K, the resonant small-signal absorption coefficient of the ^{154}Sm transition was measured to be 0.03 cm^{-1}; from this value a ^{154}Sm number density of 4×10^{12} cm^{-3} can be estimated.[29] The total Sm number density then yields 5×10^{13} cm^{-3}, which corresponds to a Sm-Sm collision rate of approximately 10^4 s^{-1} assuming a hard-sphere model.[28]

At a cell temperature of 1000 K the width of the Doppler-broadened transition amounts to $ku = 2\pi \times 580$ MHz; the homogeneous optical linewidth [half width at half maximum (HWHM)] is $2\pi \times 230$ kHz according to the lifetime (340 ns) of the excited $^7F_0$ state.[30] The pressure broadening of the homogeneous optical linewidth was measured in the case of Ar perturbers resulting in a pressure-broadening coefficient of about $2\pi \times 19$ kHz/Pa.[31] It can be assumed that the corresponding broadening coefficients for the other rare-gas perturbers are of the same order of magnitude.

The Sm vapor was contained in an aluminum-oxide ceramic tube of 1.8-cm diameter and 20-cm length with mounted brass fittings to hold the fused quartz cell windows; the windows could be rotated to allow for compensation of stress birefringence. The ceramic tube could be evacuated to 10^{-4} Pa by means of a small turbo molecular pump, which was well suited to avoid the infiltration of pump oil vapors. With this arrangement,

the Sm cell could be run continuously for about one week without refilling. For the collision studies, the pressures of the added rare-gas perturbers (He,Ne,Ar,Kr,Xe) were varied from about 30 to 500 Pa. The pressure was measured either with a thermoelectric instrument calibrated by a McLeod pressure gauge (Edwards Vacustat 2) for pressures below 100 Pa, or with a capacitance manometer (MKS Baratron 222) in the pressure range above 100 Pa. The ceramic tube was heated over a length of 6 cm by an electric ceramic oven with the heating current being pulsed in 10-ms intervals. The output of the photodetector (see below) was electronically blocked during these times in order to suppress signal contributions arising from magnetic stray fields of the heating current. The whole cell was placed between two Helmholtz coils which produced the transverse static magnetic field B. Additional coils were used to compensate for the earth's magnetic field.

3. *The detection system*

The unmodulated probe beam (see Fig. 2) was polarized parallel to the magnetic field B. Behind the sample cell the probe field and the orthogonally polarized Raman sidebands passed through a $\lambda/4$ plate which was carefully aligned to yield the required phase retardation of $\pi/2$ between the probe field and the Raman sidebands. The polarization analyzer A was inserted with an angle of about 45° with respect to the z direction. With this detection scheme the FM RHS could be recorded, see Appendix B. Let us mention that due to residual optical misalignments and imperfections a fraction of about 0.3% of the corresponding AM RHS was present in the observed FM RHS; however, these additional signal contributions due to crosstalk effects were neglible under the experimental conditions considered in this paper.

The optical heterodyne beat signal was produced in a fast p-i-n diode (Centronic OSD 1-3HSA). The ac component of the photodetector signal was amplified by a 30-dB rf preamplifier and then sent through a bandpass filter (bandwidth is 2 MHz) before reaching the rf lock-in amplifier (Princeton 5202). The heterodyne beat signal was demodulated with respect to the rf frequency of the synthesizer using a typical integration time of 0.1 s; the resulting in-phase and quadrature components were sent to a minicomputer for data storage and signal averaging. Here we will only present results of the in-phase (cosine) signals.

B. Measurements

For the measurements of the sublevel resonance signals, the modulation frequency ω_M was kept fixed and the Zeeman splitting was varied by sweeping the external magnetic field B; the typical data-acquisition time for the recording of a complete resonance curve was about one minute. The measurements were performed at fixed laser frequencies lying on the lower frequency side of the inhomogeneously broadened ^{154}Sm transition; due to the large isotope shift a sublevel coherence was excited only in ^{154}Sm atoms. Before each measurement the laser frequency was tuned to the central peak of the Doppler-free resonance at $kv_0=0$ of the ^{154}Sm line. The desired frequency detuning then was adjusted with respect to this position; the laser-tuning elements were calibrated by means of the 990-MHz separation between the ^{154}Sm and ^{152}Sm isotope components. By this procedure the laser-frequency detunings could be determined with an accuracy of about 20 MHz.

In Fig. 7 typical in-phase FM RHS are shown as a function of the sublevel detuning $\Delta_M=\omega_M-\Omega_M$ with the laser frequency detuning as a parameter; here He buffer gas was added at a pressure of 70 Pa. The sublevel detuning Δ_M is given in frequency units according to the magnetic field dependence of the Zeeman splitting frequency. It can be seen clearly that the line shape of the Zeeman resonances changes drastically for increasing laser detunings Δ_E. In the case of $\Delta_E=0$ the observed RHS display a very broad resonance structure. However, if the laser is slightly detuned from the center of the Doppler profile (e.g., for $\Delta_E/2\pi=55$ MHz), the width of the resonance decreases by almost one order of magnitude and a pair of symmetrical side lobes begins to develop. For larger laser frequency detunings this characteristic line-shape pattern becomes more and more pronounced; it is accompanied by a further decrease of the resonance linewidth and of the signal amplitude. The observed line shapes thus show the typical interference pattern of Ramsey resonances. This similarity is seen most obviously in Fig. 8, which shows a particular nice FM RHS in the case of a very large laser frequency de-

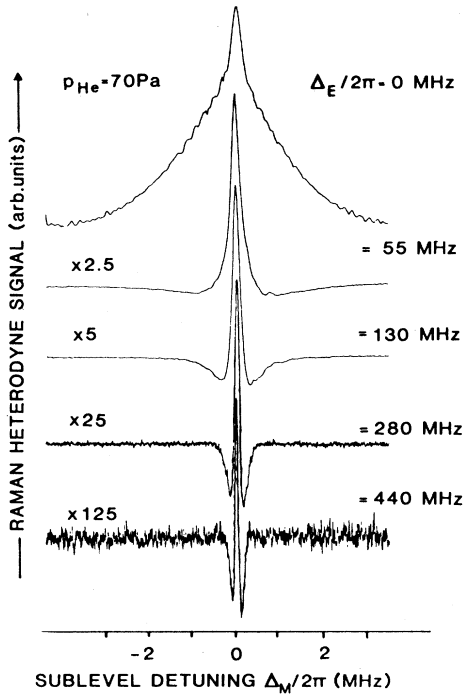

FIG. 7. Measured RHS in the case of He perturbers as a function of the sublevel detuning Δ_M for different laser detunings Δ_E, showing narrow Ramsey-type interference patterns.

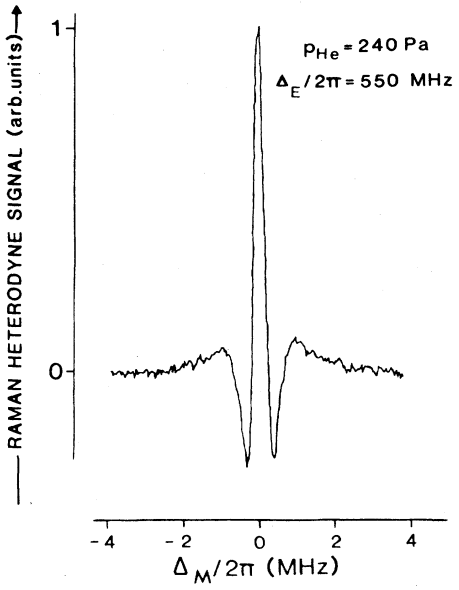

FIG. 8. Measured RHS for a relatively large laser detuning ($\Delta_E/2\pi = 550$ MHz) and a long signal averaging time, showing a pronounced Ramsey-type resonance.

tuning; here again, He was used as a buffer gas.

Within the investigated pressure range, the basic RHS line-shape features remain qualitatively the same for the different rare-gas species. The Ramsey-type interference pattern, however, is less pronounced for the heavier rare gases; as an example given, we show in Fig. 9 RHS obtained with Ar perturbers at a pressure of $p_{Ar} = 70$ Pa. In this context it is important to note that for $\Delta_E \geq 50$

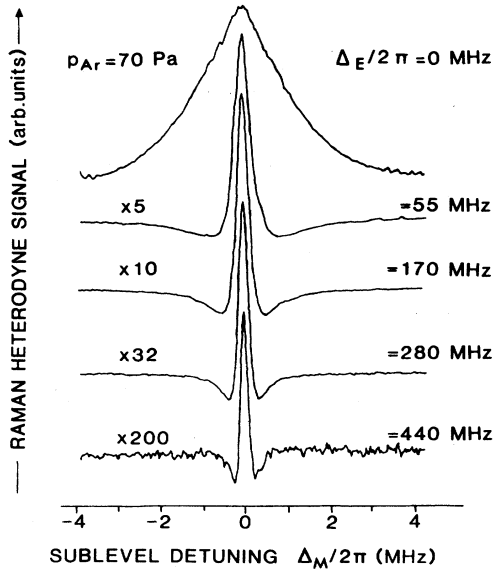

FIG. 9. Measured RHS in the case of Ar perturbers as a function of the sublevel detuning Δ_M for different laser frequency detunings Δ_E.

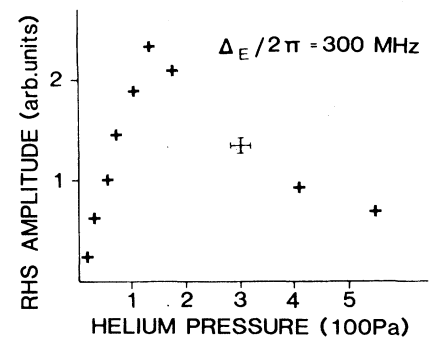

FIG. 10. Pressure dependence of the RHS amplitude for a nonzero laser detuning $\Delta_E/2\pi = 300$ MHz.

MHz the separation in velocity space between the interaction zones of the pump and probe fields clearly exceeds the width of the optically excited velocity subgroup, even if the optical pressure broadening and the laser bandwidth is taken into account.

The important role of collisions for the generation of the RHS becomes evident by considering the pressure dependence of the RHS amplitude. A typical result for He perturbers is shown in Fig. 10; during this measurement the laser detuning was kept fixed at $\Delta_E/2\pi = 300$ MHz. At first, the RHS amplitude increases with increasing buffer-gas pressure; it subsequently approaches a maximum value at a certain pressure and finally decreases again.

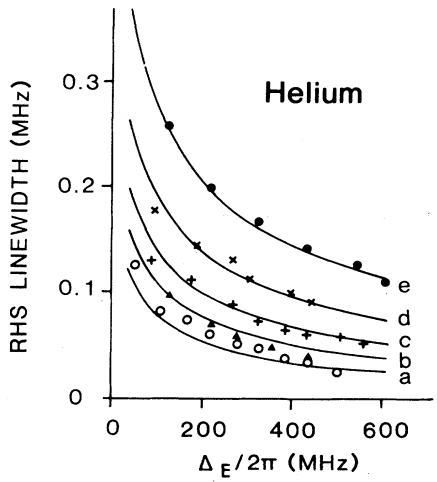

FIG. 11. RHS linewidths [half width at half maximum (HWHM)] as a function of the laser detuning Δ_E for different He pressures. The data points are measured RHS linewidths; the solid lines correspond to calculated linewidths according to the FP model (a, $p_{He} = 30$ Pa; b, 70 Pa; c, 120 Pa; d, 210 Pa; e, 370 Pa). Only two independent parameters were used to calculate the whole set of curves; the parameter values have been obtained from least-squares fits of the corresponding RHS line shapes: $c_{th} = 1.75 \times 10^3/(\text{s Pa})$ and $c_{col} = 3.0 \times 10^3/(\text{s Pa})$.

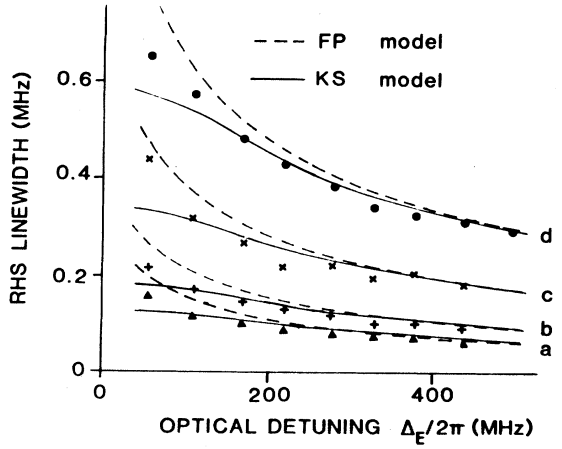

FIG. 12. RHS linewidth (HWHM) as a function of the laser detuning Δ_E for different Ar pressures (a, $p_{Ar}=40$ Pa; b, 70 Pa; c, 155 Pa; d, 290 Pa). The data points correspond to measured linewidths, the solid and dashed lines are related to overall least-squares fits of the RHS line shapes according to the KS- and FP-collision models, respectively. In the case of the KS model three free parameters were used [$c_{col}=12.3\times10^3$/(s Pa); $c_{VCC}=27\times10^3$/(s Pa); $\alpha=0.87$]; the fits based on the FP calculation were performed with the use of only two adjustable parameters [$c_{col}=11.0\times10^3$/(s Pa) and $c_{th}=5.9\times10^3$/(s Pa)].

From Figs. 7 and 9 we have seen qualitatively that the RHS linewidth decreases with increasing laser frequency detuning; this is shown on a quantitative base in Figs. 11 and 12 where the measured RHS linewidths are displayed as a function of laser detuning for different pressures of He and Ar perturbers, respectively.

V. DISCUSSION

This section contains an interpretation of the measured RHS by making use of the theoretical predictions derived in Sec. III. We first give a qualitative explanation of the observed RHS properties and then present the results of a quantitative comparison between measured and calculated RHS line shapes. It will be shown that the Fokker-Planck approach yields a good description of the collisional velocity diffusion of Sm atoms in the presence of light perturbers, whereas, for the heavier rare gases, the more complex Keilson-Storer collision model gives a better fit to the experimental data. We finally discuss the most suitable values for the different model parameters, which have been derived by fitting the predicted line shapes to the measured ones.

A. Qualitative considerations

The experimental curves can be analyzed by recalling some results of the theory, which essentially predicts that the sublevel resonance line shape can in general be written as a Fourier transform of a certain function $F(t)$, see Eqs. (3.25a) and (3.25b). This function $F(t)$ describes the distribution of diffusion times of atoms with Zeeman coherence moving from $-v_0$ to $+v_0$, and it can obviously be obtained from the measured signals by a simple Fourier transformation according to

$$F(t)=\frac{1}{\pi}\int_{-\infty}^{\infty} d\Delta_M S_{in}(\Delta_M)\cos(\Delta_M t)\ . \tag{5.1}$$

In this way a temporal resolution of the velocity-diffusion process is achieved. When the Fourier transformation (5.1) is applied to a typical set of measured curves partly shown in Fig. 7, the data points (+) shown in Fig. 13 are obtained. These Fourier transforms obviously demonstrate that the most probable as well as the mean diffusion time get larger for an increasing laser detuning, i.e., for a larger separation between the interaction zones of the pump and probe fields in velocity space. Particularly for large laser detunings the Fourier transforms show that there are barely any signal contributions arising a short time after the excitation; it takes a certain time until the first Sm atoms "arrive" at the opposite velocity subgroup $+v_0$. Due to this "intrinsic" time delay between excitation and detection process and due to the phase-sensitive detection scheme, the resonance line shapes show the observed Ramsey-type interference structure connected with the linewidth narrowing.

The relative heights of the Fourier transforms (or, equivalently, of the measured RHS) indicate that the number of atoms contributing to the RHS is strongly reduced at large detunings Δ_E; first, the number of atoms that had been excited initially is reduced according to

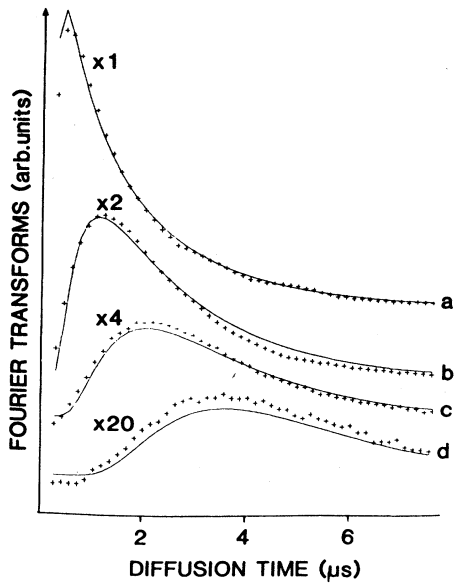

FIG. 13. Typical distribution of diffusion times of atoms with Zeeman coherence in a He atmosphere ($p_{He}=70$ Pa) for different laser detunings (a, $\Delta_E/2\pi=55$ MHz; b, 130 MHz; c, 220 MHz; d, 360 MHz). The data points are obtained by a Fourier transformation of the measured RHS; the solid lines correspond to an overall fit based on the FP model. The values for the fit parameters are $\gamma=6.0\times10^5$/s and $\gamma_{th}=1.4\times10^5$/s.

the Doppler factor and, more important, the amount of detectable sublevel coherence is decreased due to the exponential decay during the larger diffusion time.

Up to now we have omitted a discussion of the experimentally observed very broad sublevel resonance structures for zero laser frequency detuning, see Figs. 7 and 9. It is necessary to keep in mind that the theory developed in Sec. III cannot be applied to the particular case of $\Delta_E=0$, since the theoretical derivations were based on the assumption that the laser detuning Δ_E is much larger than the homogeneous optical linewidth Γ.[32] Nevertheless, it is possible to give an intuitive explanation: for $\Delta_E=kv_0=0$ both pump and probe fields interact in principle with the same atomic velocity subgroup of width Γ/k. Velocity-changing collisions with a velocity change Δu being larger than Γ/k will push the Sm atoms out of the optically excited subgroup, or, equivalently, out of the interaction region in velocity space. This limits the time of observation of the active atoms; as a consequence, the corresponding resonance linewidth broadens. The resonance structure for $\Delta_E=0$ can thus be understood as a transit-time broadening in velocity space; similar effects have already been observed and analyzed in velocity-selective rf laser double-resonance experiments.[18]

Let us finally discuss the pressure dependence of the RHS amplitude obtained for a nonzero laser detuning, see Fig. 10. The observed behavior can be understood by considering the pressure dependence of both the VCC rate γ_{VCC} and of the rate γ; the latter one describes the losses of sublevel coherence due to depolarizing collisions (γ_{col}) and due to the spatial diffusion of the atoms out of the laser beam (γ_{tr}),

$$\gamma_{\mathrm{VCC}}=c_{\mathrm{VCC}}p \ , \tag{5.2a}$$

$$\gamma=\gamma_{\mathrm{tr}}+\gamma_{\mathrm{col}}=\gamma_{\mathrm{tr}}+c_{\mathrm{col}}p \ . \tag{5.2b}$$

Here, for simplicity, we have neglected an explicit pressure dependence of γ_{tr}. If the buffer-gas pressure is increased starting from the value $p=0$, the RHS tend to become larger, since the effective number $n=\gamma_{\mathrm{VCC}}/\gamma$ of VCC within the lifetime of the sublevel coherence gets larger. For further increased pressure, however, the number of collisions contributing to the signal approaches the finite value $n=c_{\mathrm{VCC}}/c_{\mathrm{col}}$, while the damping rate γ still continues to grow. Hence the RHS amplitude decreases again after passing through a distinct maximum (see Fig. 10).

It should be pointed out that the initial increase of the RHS amplitude at low pressures is *not* due to an increasing generation of sublevel coherence as is, e.g., the case for the collision-induced sublevel resonances observed by Zou and Bloembergen.[33] In our case the sublevel coherence is produced by the modulated pump beam even for zero pressure, but it is not detectable since collisions are needed to provide for a transport in velocity space.

B. Numerical calculations

In order to analyze our experimental data on a quantitative base, we tried to fit the phenomenological-model line shapes, derived in Sec. III, to the measured sublevel resonance line shapes. These fitting attempts should provide us with more detailed information about the Sm–rare-gas collision processes or, at least, a fairly consistent set of parameters characterizing the observed collision data. Thus these fits may also serve as a test of the specific validity of the two employed collision models, i.e., of the FP model and of the KS collision model, respectively. Since in the case of the FP model the calculation of the signal line shape demands a time-consuming numerical integration according to Eq. (3.25a), we performed the least-squares fits by using the more tractable Fourier transforms $F(t)$, given either by Eq. (3.30) or by Eqs. (3.26) and (3.36), together with the corresponding Fourier transforms of the measured signals. Furthermore, we disregard in the fits the sublevel resonances observed for zero laser frequency detuning, because our theory does not include this particular case.

1. Fokker-Planck model

It can be seen from Eq. (3.30) that in the case of the FP description the theoretical signal line shape depends on the three quantities γ, γ_{th}, and v_0/u; the two rates γ and γ_{th} were taken as variable fit parameters. For v_0/u we used the measured laser frequency detuning being normalized to the calculated Doppler width $ku=2\pi\times 580$ MHz.

Let us first discuss the case where He was added as a buffer gas. The fits of the Fourier transforms $F(t)$ indicate that a single sublevel resonance curve can be well described by the FP model; the deviations of the fitted curve from the measured one typically lie within the experimental uncertainties. If the fit procedure is applied to different sublevel resonance curves that all were recorded at the same He pressure but with different laser frequency detunings, the values obtained for the free parameters γ and γ_{th} vary to within 20% around a certain mean value; no indication for a velocity dependence of γ or γ_{th} is found. This behavior is consistent with our theory which is based on the assumption that all rate constants are velocity independent.

If several theoretical curves are fitted simultaneously to such a set of sublevel resonance curves by using the same fit values for all curves (overall fit), the deviations between the theoretical and experimental curves are considerably larger, but still acceptable. One example is shown in Fig. 13, where the solid lines represent the result of the overall fit and the crosses are the corresponding experimental data points. The residual discrepancies are due to some extent to the uncertainty in the experimental determination of the laser detuning Δ_E; this mainly results in a corresponding deviation of the measured signal amplitude from the calculated one. We have performed similar least-square fits for other sets of measurements recorded at different He pressures; in this way we have obtained the pressure dependence of the two model parameters γ and γ_{tr}. The corresponding results are displayed in Fig. 14 which clearly shows the predicted linear pressure dependence of $\gamma=\gamma_{\mathrm{tr}}+c_{\mathrm{col}}p$ and $\gamma_{\mathrm{th}}=c_{\mathrm{th}}p$. We note that the value obtained for $\gamma_{\mathrm{tr}}=\gamma$ $(p=0)$ compares well with the expected transit-time broadening due to the finite laser-beam diameter.

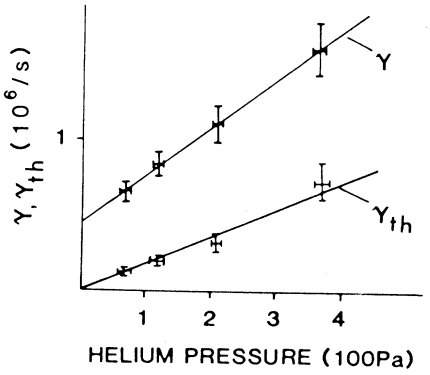

FIG. 14. Relaxation rate γ and FP parameter γ_{th} as a function of He pressure showing the expected linear pressure dependence of both rates; the solid lines are a guide for the eye.

With the use of the fitted broadening coefficients c_{col} and c_{th} we have also calculated the linewidth of the sublevel resonances for the various He pressures used in the experiment. The result of this calculation is displayed in Fig. 11 together with the experimental data points; it can be seen that the observed decrease of the RHS linewidth with increasing laser detuning is properly described by our simple theory within the entire investigated pressure range.

This good agreement between theory and experiment demonstrates that the FP-collision model allows a satisfactory description of the collision data in the case of He perturbers. The situation changes, however, for the heavier rare gases; the fit values obtained for γ and γ_{th} show systematic variations instead of being constant for different laser frequency detunings. If overall fits as in the case of He perturbers are performed, the discrepancies between the theoretical and experimental curves are unacceptably large; in fact, the deviations are much larger than the error bars. Some examples of fitting results obtained in the case of Ar perturbers are shown in Fig. 15; obviously, the FP model (left row) fails to describe the collisional velocity diffusion of Sm atoms in the presence of rare gases heavier than He.

These findings are confirmed by comparing the measured RHS linewidths with those values that are calculated with the use of the FP fit parameters; the FP model yields RHS linewidths that, especially for small laser detunings, are larger than the experimental ones, see Fig. 12.

2. *Keilson-Storer model*

In order to obtain a better description of the experimental data, we also performed fitting attempts based on the KS collision model, see Sec. III C 4. However, when the KS model was applied in the fitting procedure, one difficulty became obvious: for just a single sublevel resonance curve, the fitted values for the free parameters γ, γ_{VCC}, and α were not well defined; as one example given, a higher value for the collision rate γ_{VCC} could be compensated for by some lower value of the collisional velocity change $\Delta u = u(1-\alpha^2)^{1/2}$ without a significant change of the calculated signal line shape.

In order to overcome these difficulties, we tried to fit suitable KS line shapes simultaneously to a whole set of measurements that had been recorded under the same experimental conditions as laser intensity, Sm number density, and buffer-gas species, but with different laser detunings and with different buffer-gas pressures. As parameters we used the KS quantity α and the pressure-broadening coefficients for depolarizing and velocity-changing collisions, c_{col} and c_{VCC}, respectively.

This fitting procedure was applied in the case of the rare-gas species Ne, Ar, Kr, and Xe, and it turned out to work better. The calculated fits demonstrate that the KS model yields a more accurate description of the experimental results than the FP model. This can be seen clearly in Fig. 15, where the KS results and the above-mentioned FP fit results are displayed together with the experimental findings for the case of Ar perturbers. Moreover, the KS model also gives a better description of the measured RHS linewidths than the FP model as is indicated in Fig. 12. However, the KS model does not provide a satisfactory description of the experimental data in the case of small laser detunings, where the calculated RHS linewidths are generally too small compared with the observed ones.

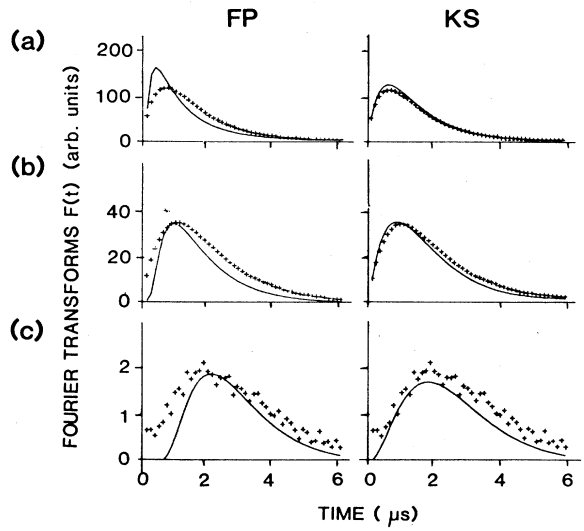

FIG. 15. Distribution of diffusion times of Zeeman coherence in the presence of Ar perturbers ($p_{Ar}=40$ Pa) for different laser detunings [(a), $\Delta_E/2\pi=110$ MHz; (b), 220 MHz; (c), 440 MHz]. The data points are obtained by a Fourier transformation of the measured RHS; the solid lines correspond to overall fits based on the KS and FP collision model, respectively. The three curves on the left side show the results obtained with the FP model, whereas the right column displays the fits according to the KS model. The numerical values for the different model parameters are the same as given in Fig. 12.

The pronounced failure of the FP description of the velocity diffusion of Sm atoms in the presence of the heavier rare gases is not that surprising; with the knowledge of the collision rate γ_{VCC} obtained from the fit with the KS model, we can easily check the validity of the preassumptions made in the Fokker-Planck approximation. In particular, the basic requirement of $\gamma_{VCC}t \gg 1$ for all considered times t cannot be met. Consider, e.g., the distribution of diffusion times for a 40-Pa Ar pressure shown in Fig. 15. In this case the characteristic diffusion time is about 1 μs; with the use of the value for the collision rate γ_{VCC} obtained from the fit with the KS model, the quantity $(\gamma_{VCC}t)$ only yields a value around unity.

3. *Fit results*

Table I contains the calculated values for the different model parameters that have given the best overall agreement of fitted and measured RHS.

The derived rates for depolarizing and velocity-changing collisions are given in terms of the corresponding cross sections σ_{col} and σ_{VCC} according to the relation $\gamma = N_p v_r \sigma$; here N_p is the perturber density and v_r is the mean relative velocity of active and perturber atoms,

$$v_r = \left[\frac{8k_B T}{\pi} \left[\frac{1}{m_A} + \frac{1}{m_p} \right] \right]^{1/2} . \tag{5.3}$$

An interpretation of the obtained data is possible by comparing them with appropriate hard-sphere values and with corresponding values that have been derived previously in a rf laser double-resonance experiment.[18] The hard-sphere cross sections $\sigma_{HS} = \pi(r_A + r_p)^2$ were derived with the use of the tabulated values for the atomic radii;[34] the values for the parameters α_{HS} characterizing the width of the hard-sphere collision kernel are determined by the mass ratio of perturber and active atoms.[35,36]

To start with, we discuss the fit results in the case of He perturbers. In Table I the fitted pressure-broadening coefficient c_{th} of the FP thermalization rate $\gamma_{th} = c_{th}p$ is given in its reciprocal value $1/c_{th}$; this allows a simple interpretation: $1/c_{th}$ in units of (s Pa) gives the characteristic time required for the thermalization of a given atomic velocity anisotropy in a He atmosphere of pressure $p = 1$ Pa. The errors in the determination of c_{th} and of the cross section σ_{col} are about 20% as can be estimated from the slopes of the curves displayed in Fig. 14. The FP parameter γ_{th} is directly related to transport coefficients in classical transport theory; a knowledge of this quantity yields, e.g., the value for the diffusion coefficient $D = (k_B T)/(m_A \gamma_{th})$.[24] Similar relationships between the usual description of collision processes in laser spectroscopy in terms of collision kernels and collision rates and the description of collision processes in classical transport theory using transport coefficients of diffusion, viscosity, and thermal conductivity, have been discussed recently in detail.[37]

In the case of the heavier rare-gas perturbers, we have listed in Table I the fit results obtained with the KS model. Let us mention that the values for the KS parameters α and σ_{VCC} are first estimates; we cannot give standard deviations since the values were obtained by fitting all measured curves simultaneously. Nevertheless, it is possible to provide some insight into the collisional redistribution processes. The values in Table I indicate that our values for α are systematically larger than those obtained with a hard-sphere collision model; i.e., the mean collisional velocity change of the Sm atom (with the orientation being preserved) is clearly smaller than expected from the hard-sphere model. This fact can be interpreted if the fitted values for the cross sections σ_{col} of collisional depolarization are taken into account. Especially in the case of the heavier rare gases, the values for σ_{col} approach the hard-sphere cross sections σ_{HS}. This indicates that collisions with small impact parameters ("hard-sphere" or "strong" collisions) result in a depolarization rather than in a thermalization of the considered multipole component. In contrast, the atomic orientation is merely preserved by weak collisions with large impact parameters resulting in relatively small velocity changes.

Since we have confined our analysis of the experimental data to the case of a nonzero laser frequency detuning ($\Delta_E/2\pi \gtrsim 50$ MHz), our fitting attempts are mainly sensitive to the relatively broad part of the collision kernel; we cannot account for the very small velocity changes associated with very weak "diffractive" collisions. In contrast, the above-mentioned rf laser double-resonance experiment[18] was merely sensitive to VCC with relatively small velocity changes; there, the velocity resolution was determined by the width of the homogeneous optical line. Since a KS model has been applied to describe the observed collision data in this rf

TABLE I. Best-fit values for the various collision parameters. For comparison, the hard-sphere values α_{HS} and σ_{HS} are also displayed.

Perturber	Model	σ_{col} (Å^2)	σ_{VCC} (Å^2)	σ_{HS} (Å^2)	$1/c_{th}$ (μs Pa)	α	α_{HS}
He	FP	1.8		28	570		
Ne	KS	10	32	30		0.90	0.84
Ar	KS	21	46	36		0.87	0.67
Kr	KS	32	58	41		0.88	0.51
Xe	KS	40	95	47		0.90	0.35

laser double-resonance experiment, a comparison of the values for the KS model parameters obtained in that experiment with the corresponding values presented here should serve as a test of the adequacy of the KS kernel to describe both the small- and the large-angle scattering processes. It turns out that our values for σ_{VCC} are smaller by a factor of 4 to 7, whereas the values for the mean velocity change Δu per collision are considerably larger than those obtained in Ref. 18. Obviously, a KS kernel cannot provide a proper description of the whole velocity scattering spectrum. If the KS-model parameters are adjusted to describe the broad part of the physical collision kernel, the effects of small-angle scattering processes cannot be reproduced, and vice versa. Since the small-angle scattering processes strongly contribute to the total scattering cross section,[38] it is not surprising that the values for σ_{VCC} obtained in Ref. 18 are larger than the values measured in the experiment considered here. In Ref. 7 we have estimated the number $n=\gamma_{VCC}/\gamma_{th}$ of collisions that are necessary for a thermalization of a given atomic velocity anisotropy; since we used the values for γ_{VCC} obtained in Ref. 18, these numbers n have been overestimated.

This result indicates that a two-term kernel consisting of a relatively broad part and a narrow component should give a better description of the observed collision data. Recently, other VCC experiments have given also evidence for such a two-term kernel,[39,40] and in some cases a two-term kernel has been applied successfully to describe the whole velocity scattering spectrum.[40,41]

Another difference between the experiment considered here and the rf laser double-resonance experiment might play an important role for the interpretation of the cross sections for depolarizing collisions; in Ref. 18 the relaxation of the alignment of the $J=1$ ground state of Sm was studied, whereas this paper considers the relaxation of the orientation. A comparision of the measured values shows that the cross sections for the collisional relaxation of the orientation are significantly larger than those for the relaxation of the alignment; the ratio of both cross sections yields 1.3 for He, 1.6 for Ar, and 2.5 for Xe.

These measured cross sections for the collisional relaxation of the orientation and alignment in the $J=1$ ground state of Sm can be compared with other measurements of these quantities. To start with, the alignment relaxation rate was measured recently for Ar perturbers;[42] the determined value differs only by 20% from the corresponding value measured in the rf laser double-resonance experiment.[18] However, the cross sections measured by use of collision-induced Hanle resonances in four-wave light mixing[33] differ drastically from our values; Zou and Bloembergen reported values for σ_{col} that are smaller by a factor of about 50 compared with our results. In this respect, let us point out that in the vicinity of the considered $J=1-J'=0$ Sm transition at $\lambda=570.68$ nm there are two other Sm lines ($J=2-J'=3$ and $J=3-J'=2$) with an optical frequency separation of only -45 GHz and $+50$ GHz from the $J=1-J'=0$ line, respectively.[43] Since the method used in Ref. 33 utilizes optical frequency detunings of 10–20 GHz, signal contributions arising from these other Sm transitions cannot be excluded. In contrast, our method utilizes optically *resonant* Raman processes and is thus capable to distinguish between the various Sm lines. Here we just mention that we have also performed measurements of σ_{col} for the $J=3$ ground state of Sm using the $J=3-J'=2$ transition at $\lambda=570.62$ nm; in this case we found the value $\sigma_{col}=0.028$ Å^2 for He perturbers and $\sigma_{col}=0.34$ Å^2 for Ar. These cross sections agree within only 10% with those values reported in Ref. 33.

On the other hand, we cannot explain the pronounced difference between the depolarizing cross sections for the orientation and alignment in the $J=1$ ground state of Sm that have been measured in the rf laser double-resonance experiment[18] and in the experiment reported in this paper. Other measurements of the orientation and alignment relaxation rates have been performed, e.g., for the $^3P_1$ state of Yb atoms in a He atmosphere where a slightly higher relaxation rate for the orientation has been found.[12] Moreover, optical-pumping techniques have been used to measure the relaxation of the orientation and alignment in the $^3P_1$ states of Hg and Cd again in the presence of rare-gas perturbers;[44] in these experiments also a higher relaxation rate (10–20 %) for the orientation was measured. However, differences between both relaxation rates in the order of 100% seem not to have been observed so far.

In this respect let us add the following remarks. As already pointed out above, the different velocity changes studied in this work and in Ref. 18 possibly measure the depolarization due to different parts of the interaction potential. Hence, a measurement of the relaxation rate for both the orientation and the alignment using the technique described in the present work would be very helpful in the understanding of the observed differences in collisional cross sections. Since our method is capable of inducing either an orientation or an alignment in the $J=1$ ground state by a proper choice of the modulation structure of the driving pump laser beam (see Sec. III B 1), a direct measurement of both relaxation rates seems possible.

There is, however, another complication in the interpretation of our data. The $\hat{\mathbf{z}}$ axis is perpendicular to the cell, due to the applied **B** field, while the collisional perturbation has cylindrical symmetry about the laser-beam-propagation direction. Thus, for the larger-angle collisions, it cannot be excluded that some orientation is converted into alignment and vice versa due to anisotropic collisions. This conversion rate is difficult to estimate in our case; for the small-angle collisions studied in most previous experiments, the departure from spherical symmetry is small and not very important.[45] If only orientation would be detected in our experiment the conversion rate might appear as a loss or destruction rate. Our RHS, however, contain contributions of both the transverse orientation and of the alignment [see Eq. (B10)]. Thus the detection scheme does not allow us to measure the orientation and alignment separately; as a consequence, no conclusions on a possible conversion of orientation into alignment can be derived from measure-

ments using the present technique.

VI. SUMMARY

We have reported on the observation of collision-induced Ramsey resonances in atomic Sm vapor in the presence of rare-gas perturbers. The formation of these resonances is due to the collisional diffusion of Sm atoms in velocity space. The observation of this phenomenon is made possible by use of both a velocity-selective excitation and detection scheme for oscillating Zeeman coherence in the $J=1$ ground state of Sm. If the Zeeman coherence is excited and detected in different velocity subgroups the measured RHS shows the characteristic features of Ramsey-type resonances; we have observed the typical interference pattern as well as the narrowing of the resonance linewidth even below the limit given by the time rate for depolarizing collisions and the transit-time broadening.

The theoretical description of this novel Ramsey interference effect is based on a steady-state perturbation solution of the density-matrix equations for a Zeeman-split $J=1-J'=0$ transition. The collisional velocity diffusion of the $|\Delta m|=1$ Zeeman coherence has been taken into account by means of a classical transport equation. Under certain approximations a very simple, model-independent RHS line-shape expression could be derived; the calculated RHS line shape turned out to be sensitive to both depolarizing and velocity-changing collision effects. This theoretical result has enabled us to obtain the *temporal evolution* of the collisional-diffusion process by means of a simple Fourier transformation of the measured RHS. We have shown that this novel way of studying VCC is due to the well-defined phase sensitivity of the Raman heterodyne detection of the atomic coherence.

A direct comparison of the measured temporal evolution of the velocity-diffusion process with corresponding theoretical predictions based on a Fokker-Planck model and on a Keilson-Storer collision model enabled us to test the specific validity of these two approaches. It turned out that the velocity thermalization of Sm atoms in a He atmosphere can be described properly within the investigated He pressure range by means of the Fokker-Planck approximation; the comparison has given the corresponding time constant for the collisional thermalization. However, the Fokker-Planck model failed to describe the velocity diffusion of Sm atoms in the presence of heavier rare-gas perturbers; here the phenomenological Keilson-Storer kernel has produced a better agreement with the experimental data. These fitting attempts yielded numerical values for the different model parameters; in particular, we derived cross sections for depolarizing and velocity-changing collisions associated with the transverse orientation of the $J=1$ Sm ground state.

For simplicity, we have confined our analysis of the experimental data to the case of a relatively large separation in velocity space between the two interaction zones that are defined by the pump and probe laser field, respectively. Therefore diffractive small-angle scattering effects resulting in small collisional velocity changes of the active atoms were not taken into account. However, a comparison of the measured cross sections for VCC with the results of a previously performed rf laser double-resonance experiment[18] has given evidence for a two-term collision kernel; in order to provide a consistent description of the collisional data in the rf laser experiment and in our experiment, this two-term kernel should consist of a narrow part describing small-angle scattering processes and of a broad part taking into account large-angle scattering effects.

Our technique has to be compared with other methods used for the study of VCC concerning multipole moments in a J-state manifold. Like other steady-state experiments, our method cannot resolve collisional velocity changes resulting in a Doppler shift of less than the homogeneous optical linewidth; here, the currently developed stimulated photon-echo experiments can yield higher velocity resolution.[13,14] On the other hand, our method clearly extends previous velocity-selective optical pumping (VSOP) techniques[11] since it allows us to obtain a temporal resolution of the elastic collision effects.

Moreover, our method is capable of studying velocity-redistribution processes associated with a transverse orientation or with a transverse alignment; we have shown that a velocity-selective excitation of either the orientation or the alignment is possible if the modulation structure of the driving pump laser field is chosen properly. Thus, it seems obvious that Raman heterodyne Ramsey spectroscopy in velocity space may have useful applications in collision studies and sublevel coherence spectroscopy.

ACKNOWLEDGMENTS

We are indebted to Chr. Tamm and P. Berman for helpful discussions. One of us (E.B.) acknowledges support by the Niedersächsische Graduiertenförderung and another of us (J.M.) by the Heisenberg-Programm of the Deutsche Forschungsgemeinschaft.

APPENDIX A

Here we present a second-order steady-state perturbation treatment of the density-matrix equations (3.7) to derive analytic expressions describing the excitation of $\Delta m=1$ ground-state Zeeman coherence. With the use of the field-interaction representation

$$\rho_{14}=\tilde{\rho}_{14}e^{i\omega_+ t-ik_+ x}, \tag{A1a}$$

$$\rho_{24}=\tilde{\rho}_{24}e^{i\omega_E t-ikx}, \tag{A1b}$$

$$\rho_{34}=\tilde{\rho}_{34}e^{i\omega_- t-ik_- x}, \tag{A1c}$$

$$\rho_{21}=\tilde{\rho}_{21}e^{-i\omega_M t+i(k_+-k)x}, \tag{A1d}$$

$$\rho_{32}=\tilde{\rho}_{32}e^{-i\omega_M t+i(k-k_-)x}, \tag{A1e}$$

$$\rho_{31}=\tilde{\rho}_{31}e^{-2i\omega_M t+i(k_+-k_-)x}, \tag{A1f}$$

we obtain in the rotating-wave approximation the following equations of motion for the nondiagonal density-matrix elements:

$$\frac{\partial}{\partial t}\tilde{\rho}_{24}=[i(kv_0+kv)-\Gamma_E]\tilde{\rho}_{24} +i\alpha_\pi(\rho_{44}-\rho_{22})+\alpha_\sigma(\tilde{\rho}_{21}+\tilde{\rho}_{23}) , \tag{A2a}$$

$$\frac{\partial}{\partial t}\tilde{\rho}_{14}=[i(kv_0+kv-\Delta_M)-\Gamma_E]\tilde{\rho}_{14} -\alpha_\sigma(\rho_{44}-\rho_{11})-i\alpha_\pi\tilde{\rho}_{12}+\alpha_\sigma\tilde{\rho}_{13} , \tag{A2b}$$

$$\frac{\partial}{\partial t}\tilde{\rho}_{34}=[i(kv_0+kv+\Delta_M)-\Gamma_E]\tilde{\rho}_{34} -\alpha_\sigma(\rho_{44}-\rho_{33})-i\alpha_\pi\tilde{\rho}_{32}+\alpha_\sigma\tilde{\rho}_{31} , \tag{A2c}$$

$$\frac{\partial}{\partial t}(\tilde{\rho}_{21}+\tilde{\rho}_{32})=(i\Delta_M-\gamma_{\rm tr})(\tilde{\rho}_{21}+\tilde{\rho}_{32}) -\alpha_\sigma^*\tilde{\rho}_{24}-\alpha_\sigma\tilde{\rho}_{42}+i\alpha_\pi(\tilde{\rho}_{41}-\tilde{\rho}_{34}) , \tag{A2d}$$

$$\frac{\partial}{\partial t}(\tilde{\rho}_{21}-\tilde{\rho}_{32})=(i\Delta_M-\gamma_{\rm tr})(\tilde{\rho}_{21}-\tilde{\rho}_{32}) -\alpha_\sigma^*\tilde{\rho}_{24}+\alpha_\sigma\tilde{\rho}_{42}+i\alpha_\pi(\tilde{\rho}_{41}+\tilde{\rho}_{34}) , \tag{A2e}$$

$$\frac{\partial}{\partial t}\tilde{\rho}_{31}=(2i\Delta_M-\gamma_{\rm tr})\tilde{\rho}_{31}-\alpha_\sigma\tilde{\rho}_{41}-\alpha_\sigma^*\tilde{\rho}_{34} . \tag{A2f}$$

Here we have ignored the slight difference of k vectors of the carrier and sidebands, i.e. we have assumed $k_+\approx k_-\approx k$; in fact, under our experimental conditions $(k-k_-)/k$ only is about 10^{-7}. The detuning parameters are defined by

$$kv_0=\Omega_E-\omega_E , \tag{A3a}$$

$$\Delta_M=\omega_M-\Omega_M . \tag{A3b}$$

The first three equations (A2a)–(A2c) describe the behavior of the "optical" coherences, whereas the equations (A2d)–(A2f) are related to the evolution of the magnetic Zeeman coherences. In these last three equations we have written the Zeeman coherences in terms of the standard tensor components of the density-matrix elements;[44] in particular, the linear combinations $(\tilde{\rho}_{21}+\tilde{\rho}_{32})$ and $(\tilde{\rho}_{21}-\tilde{\rho}_{32})$ are related to the transverse orientation $\tilde{\rho}_1^1$ and the transverse alignment $\tilde{\rho}_1^2$, respectively,

$$\tilde{\rho}_1^1=(\tilde{\rho}_{21}+\tilde{\rho}_{32})/\sqrt{2} , \tag{A4a}$$

$$\tilde{\rho}_1^2=(\tilde{\rho}_{21}-\tilde{\rho}_{32})/\sqrt{2} . \tag{A4b}$$

In the equations of motion (A2a)–(A2f) we have specified the phenomenological relaxation terms. Here $\gamma_{\rm tr}$ describes the decay of the ground-state density-matrix elements ρ_{ij} $(i,j=1,2,3)$ towards thermal equilibrium; this rate $\gamma_{\rm tr}$ is given by the transit time of the atoms through the laser beam. The optical coherences ρ_{14}, ρ_{24}, and ρ_{34} are assumed to decay with a rate Γ_E. We have not explicitly specified the equations of motion for the level populations ρ_{ii}, as they are not required in the following low-order perturbation calculation for the sublevel coherence under consideration.

In first-order perturbation treatment the excitation of the optical coherences is described by

$$\tilde{\rho}_{14}=\frac{-\alpha_\sigma(\rho_{44}-\rho_{11})}{-i(kv_0+kv-\Delta_M)+\Gamma_E} , \tag{A5a}$$

$$\tilde{\rho}_{24}=\frac{i\alpha_\pi(\rho_{44}-\rho_{22})}{-i(kv_0+kv)+\Gamma_E} , \tag{A5b}$$

$$\tilde{\rho}_{34}=\frac{-\alpha_\sigma(\rho_{44}-\rho_{33})}{-i(kv_0+kv+\Delta_M)+\Gamma_E} . \tag{A5c}$$

The denominators in (A5a)–(A5c) reflect the optical resonance conditions for the carrier and sidebands of the modulated laser field. If the considered sublevel detunings Δ_M are small compared to the homogeneous optical linewidth Γ_E, all optical fields interact with the same group of atoms and we can ignore the detunings Δ_M in the Eqs. (A5a)–(A5c). With this assumption we obtain, e.g., for $\tilde{\rho}_1^1$ the following second-order perturbation solution:

$$(-i\Delta_M+\gamma_{\rm tr})\tilde{\rho}_1^1(v) =\frac{i\alpha_\pi}{\sqrt{2}}\left[c_1\frac{\Gamma_E}{(kv_0+kv)^2+\Gamma_E^2}+ic_2\frac{kv_0+kv}{(kv_0+kv)^2+\Gamma_E^2}\right] \tag{A6a}$$

with c_1 and c_2 given by

$$c_1=\alpha_\sigma(2\rho_{44}-\rho_{33}-\rho_{22}) -\alpha_\sigma^*(2\rho_{44}-\rho_{11}-\rho_{22}) , \tag{A6b}$$

$$c_2=\alpha_\sigma(\rho_{22}-\rho_{33})+\alpha_\sigma^*(\rho_{22}-\rho_{11}) . \tag{A6c}$$

The first term on the right side of Eq. (A6a) reflects a velocity-selective excitation of sublevel coherence; the width of the resonance in velocity space is determined by the homogeneous optical linewidth Γ_E. In contrast to this, the second term in (A6a) describes a dispersive excitation process of sublevel coherence that yields contributions even in velocity subgroups with velocities v given by $|kv+kv_0|\gtrsim\Gamma_E$. This excitation process requires a nonzero population difference in the ground-state sublevels that can be created, e.g., by optical pumping. In order to avoid this excitation channel we have to make sure that no optical pumping takes place; this is the case if the optical transitions are coupled with equal strengths, i.e., for $|\alpha_\pi|=|\alpha_\sigma|$. With the neglect of the second term in Eq. (A6a), we finally obtain for $\tilde{\rho}_1^1(v)$ and $\tilde{\rho}_1^2(v)$

$$(-i\Delta_M+\gamma_{\rm tr})\tilde{\rho}_1^1(v) =\frac{i\alpha_\pi}{\sqrt{2}}(\alpha_\sigma^*-\alpha_\sigma)\frac{2}{3}NW(v)\frac{\Gamma_E}{(kv_0+kv)^2+\Gamma_E^2} , \tag{A7a}$$

$$(-i\Delta_M+\gamma_{\rm tr})\tilde{\rho}_1^2(v) =\frac{i\alpha_\pi}{\sqrt{2}}(\alpha_\sigma^*+\alpha_\sigma)\frac{2}{3}NW(v)\frac{\Gamma_E}{(kv_0+kv)^2+\Gamma_E^2} . \tag{A7b}$$

Here we have used the values for the level populations in thermal equilibrium

$$\rho_{44}=0,\ \rho_{11}=\rho_{22}=\rho_{33}=\tfrac{1}{3}NW(v)\ , \tag{A8a}$$

with $W(v)$ and u given by

$$W(v)=\frac{1}{\sqrt{\pi}u}\exp[-(v/u)^2]\ , \tag{A8b}$$

$$u=\sqrt{2k_BT/m_A}\ . \tag{A8c}$$

N is the total atomic number density and $W(v)$ describes the Maxwell velocity distribution with u being the most probable speed of the active atoms with mass m_A.

APPENDIX B

Here we briefly describe the Raman heterodyne technique to monitor atoms with oscillating sublevel coherence. For a more detailed treatment we refer the reader to the literature.[16,18]

The unmodulated probe field and the oscillating sublevel coherence give rise to the creation of frequency-shifted coherent Raman fields propagating in the same direction as the probe field (see Fig. 1). Let us first calculate these Raman fields.

The Raman polarizations can easily be determined in a first-order perturbation treatment of the corresponding density-matrix equations of motion. In the rotating-wave approximation and under steady-state conditions we obtain the following equations of motion for the elements $\tilde{\rho}_{14}$ and $\tilde{\rho}_{34}$:

$$[-i(kv_0+\epsilon kv)+\Gamma_E]\tilde{\rho}_{14}(v)=-i\alpha_p\tilde{\rho}_{12}(v)\ , \tag{B1a}$$

$$[-i(kv_0+\epsilon kv)+\Gamma_E]\tilde{\rho}_{34}(v)=-i\alpha_p\tilde{\rho}_{32}(v)\ . \tag{B1b}$$

Here we have used the same notation and have made the same assumption ($\Delta_M<\Gamma_E$) as in Appendix A. The rapidly oscillating factors have been removed by the transformation

$$\rho_{14}=\tilde{\rho}_{14}e^{i\omega_+t-i\epsilon kx}\ , \tag{B2a}$$

$$\rho_{34}=\tilde{\rho}_{34}e^{i\omega_-t-i\epsilon kx}\ . \tag{B2b}$$

The optical coherences ρ_{14} and ρ_{34} give rise to a macroscopic polarization $\mathbf{P}$

$$\mathbf{P}=\mathrm{Tr}(\boldsymbol{\mu}\cdot\langle\rho\rangle)\ , \tag{B3}$$

where the angle brackets $\langle\ \rangle$ denote the velocity integration

$$\langle\rho_{ij}\rangle=\int dv\,\rho_{ij}(v)\ . \tag{B4}$$

For an optically thin medium of length L the resulting field $\mathbf{E}$ behind the sample cell is given by

$$\begin{aligned}\mathbf{E}=&\left[\frac{E_p}{2}e^{i\omega_Et-i\epsilon kx}+\text{c.c.}\right]\hat{\mathbf{z}}\\&+\left[\frac{E_+}{2}e^{i\omega_+t-i\epsilon kx}+\text{c.c.}\right]\hat{\mathbf{y}}\\&+\left[\frac{E_-}{2}e^{i\omega_-t-i\epsilon kx}+\text{c.c.}\right]\hat{\mathbf{y}}\ .\end{aligned} \tag{B5}$$

The amplitudes $E_\pm$ of the Raman sidebands are given by[18]

$$E_+=\frac{kL}{\epsilon_0}\frac{\mu}{\sqrt{2}}\langle\tilde{\rho}_{14}\rangle \tag{B6a}$$

and

$$E_-=\frac{kL}{\epsilon_0}\frac{\mu}{\sqrt{2}}\langle\tilde{\rho}_{34}\rangle\ . \tag{B6b}$$

The orthogonally polarized probe laser field E_p and the Raman sidebands $E_\pm$ can be phase shifted by an angle θ by means of a retardation plate; behind the retardation plate all fields are projected along a common direction by a polarization analyzer that is inserted under an angle Φ with respect to the $\hat{\mathbf{z}}$ axis. The resulting heterodyne beat signal on a photodetector can be written in the form[18]

$$\begin{aligned}|E|^2_{\text{beat}}=&E_p\sin(2\Phi)\{E_p\cos\theta[\mathrm{Re}(m_{\text{AM}})\cos(\omega_Mt)+\mathrm{Im}(m_{\text{AM}})\sin(\omega_Mt)]\\&+E_p\sin\theta[\mathrm{Re}(m_{\text{FM}})\cos(\omega_Mt)+\mathrm{Im}(m_{\text{FM}})\sin(\omega_Mt)]\}\ ;\end{aligned} \tag{B7}$$

here the modulation parameters m_{AM} and m_{FM} describe a corresponding amplitude (AM) and frequency (FM) modulation of the total signal field in front of the detector with frequency ω_M. The parameters m_{AM} and m_{FM} are given by

$$m_{\text{AM}}=(E_+^*+E_-)/(2E_p)\ , \tag{B8a}$$

$$m_{\text{FM}}=-i(E_+^*-E_-)/(2E_p)\ . \tag{B8b}$$

Without a retardation plate ($\theta=0$), only the AM contribution of the total signal field yields a heterodyne beat signal; if a $\lambda/4$ plate ($\theta=\pi/2$) is inserted, the FM-modulation depth m_{FM} can be monitored.[18] With the use of a phase-sensitive detection scheme, one can further distinguish between the in-phase ($\sim\cos\omega_Mt$) and quadrature ($\sim\sin\omega_Mt$) signals.

In the FM-detection mode, the resulting in-phase and quadrature RHS (S_{in} and S_{qu}) then are given by

$$S_{\text{in}}=E_p^2\mathrm{Re}(m_{\text{FM}})\ , \tag{B9a}$$

$$S_{\text{qu}}=E_p^2\mathrm{Im}(m_{\text{FM}})\ . \tag{B9b}$$

The result (B8a) and (B8b) can be made more transparent. When we make use of the equations (A4a), (A4b), (B1a), (B1b), (B6a), and (B6b),

$$m_{\text{AM}}=\frac{kL}{\epsilon_0}\mu\frac{i\alpha_p}{2E_p}\int dv\frac{\Gamma_E\tilde{\rho}_1^2(v)-i(kv_0+\epsilon kv)\tilde{\rho}_1^1(v)}{(kv_0+\epsilon kv)^2+\Gamma_E^2}\ , \tag{B10a}$$

$$m_{\text{FM}}=\frac{kL}{\epsilon_0}\mu\frac{\alpha_p}{2E_p}\int dv\frac{\Gamma_E\tilde{\rho}_1^1(v)-i(kv_0+\epsilon kv)\tilde{\rho}_1^2(v)}{(kv_0+\epsilon kv)^2+\Gamma_E^2}\ . \tag{B10b}$$

These equations show that the Raman heterodyne signals generally contain contributions from both the transverse orientation $\tilde{\rho}_1^1$ and from the alignment $\tilde{\rho}_1^2$; each of these signal contributions is connected either with a dispersive or absorptive detection sensitivity in velocity space. However, only the absorptive detection sensitivity permits a velocity-selective detection of the sublevel coherence as indicated by the Lorentzian resonances in Eqs. (B10a) and (B10b); in this case, the main contribution to the signal stems from those atoms having a velocity $v = -\epsilon v_0$.

It is shown in Sec. III B 1 that either a transverse orientation or a transverse alignment can be created by a proper choice of the modulation structure of the exciting pump laser field. If one assumes, e.g., a frequency-modulated pump field, no transverse alignment is induced ($\tilde{\rho}_1^2 = 0$) and therefore only the RHS recorded in the FM-detection mode provide an absorptive detection sensitivity for $\tilde{\rho}_1^1$; in this way a velocity-selective detection of the sublevel coherence can be achieved, as depicted in Fig. 1.

[1]N. F. Ramsey, Phys. Rev. **78**, 695 (1950); *Molecular Beams* (Oxford University Press, London, 1963).

[2]J. E. Thomas, P. R. Hemmer, S. Ezekiel, C. C. Leiby, Jr., R. H. Picard, and C. R. Willis, Phys. Rev. Lett. **48**, 867 (1982); P. R. Hemmer, S. Ezekiel, and C. C. Leiby, Jr., Opt. Lett. **8**, 440 (1983).

[3]J. Mlynek, R. Grimm, E. Buhr, and V. Jordan, in *Fundamentals of Quantum Optics II,* edited by E. L. Ehlotzky (Springer Verlag, Heidelberg, 1987) p. 249.

[4]J. Mlynek, K. H. Drake, G. Kersten, D. Frölich, and W. Lange, Opt. Lett. **6**, 87 (1981).

[5]J. Mlynek, N. C. Wong, R. G. DeVoe, E. S. Kintzer, and R. G. Brewer, Phys. Rev. Lett. **50**, 993 (1983).

[6]Ye. V. Baklanov, V. P. Chebotaev, and B. Ya. Dubetsky, Appl. Phys. **11**, 201 (1976); M. M. Salour and C. Cohen-Tannoudji, Phys. Rev. Lett. **38**, 757 (1977); Ye. V. Baklanov, B. Ya. Dubetsky, and V. P. Chebotaev, Appl. Phys. **9**, 171 (1976); J. C. Bergquist, S. A. Lee, and J. E. Hall, Phys. Rev. Lett. **38**, 159 (1977).

[7]E. Buhr and J. Mlynek, Phys. Rev. Lett. **57**, 1300 (1986); **57**, 2332(E) (1986).

[8]See, e.g., P. R. Berman, in *New Trends in Atomic Physics,* edited by G. Grynberg and R. Stora (North-Holland, Amsterdam, 1984), Vol. 1, p. 451, and references therein.

[9]I. Colomb, M. Gorlicki, and M. Dumont, Opt. Commun. **21**, 289 (1977).

[10]M. Pinard, C. G. Aminoff, and F. Laloë, Phys. Rev. A **19**, 2366 (1977).

[11]C. G. Aminoff and M. Pinard, J. Phys. (Paris) **43**, 263 (1982).

[12]A. P. Ghosh, C. D. Nabors, M. A. Attili, J. E. Thomas, and M. S. Feld, Phys. Rev. Lett. **53**, 1333 (1984).

[13]J. C. Keller and J. L. LeGouët, Phys. Rev. A **32**, 1624 (1985).

[14]A. G. Yodh, J. Golub, and T. W. Mossberg, Phys. Rev. A **32**, 844 (1985); A. G. Yodh, T. W. Mossberg, and J. E. Thomas, *ibid.* **34**, 5150 (1986); A. P. Ghosh, C. D. Nabors, M. A. Attili, and J. E. Thomas, Phys. Rev. Lett. **54**, 1974 (1985); J. E. Thomas, A. P. Ghosh, and M. A. Attili, Phys. Rev. A **33**, 3029 (1986).

[15]P. R. Berman, Phys. Rev. A **9**, 2170 (1974).

[16]N. C. Wong, E. S. Kintzer, J. Mlynek, R. G. DeVoe, and R. G. Brewer, Phys. Rev. B **28**, 4993 (1983).

[17]J. Mlynek, Chr. Tamm, E. Buhr, and N. C. Wong, Phys. Rev. Lett. **53**, 1814 (1984).

[18]Chr. Tamm, E. Buhr, and J. Mlynek, Phys. Rev. A **34**, 1977 (1986).

[19]For an introduction to nonlinear laser spectroscopy, see, e.g., M. Levenson, *Introduction to Nonlinear Laser Spectroscopy* (Academic, New York, 1982).

[20]R. K. Raj, E. Köster, Q. F. Gao, G. Camy, D. Bloch, and M. Ducloy, in *Laser Spectroscopy VI,* edited by H. P. Weber and W. Lüthy (Springer, Heidelberg, 1983), p. 122.

[21]P. R. Berman, in *Advances in Atomic and Molecular Physics* (Academic, New York, 1977), Vol. 13, p. 74.

[22]See, e.g., in Ref. 19, p. 211.

[23]J. Keilson and A. E. Storer, Q. Appl. Math. **10**, 243 (1952).

[24]See, e.g., F. Reif, *Fundamentals of Statistical and Thermal Physics* (McGraw-Hill, New York, 1965).

[25]E. Buhr, Ph.D. thesis, Hannover University, 1987.

[26]*CRC-Handbook of Chemistry and Physics,* 55th ed. (Chemical Rubber Company, Cleveland, 1974).

[27]H. Brand and A. Steudel, Z. Phys. A **296**, 281 (1980).

[28]F. M. J. Pichanick and G. K. Woodgate, Proc. R. Soc. London, Ser. A **263**, 89 (1961).

[29]Chr. Tamm, Ph.D. thesis, Hannover University, 1986.

[30]K. H. Drake, Ph.D. thesis, Hannover University, 1986.

[31]P. Hannaford and R. M. Lowe, J. Phys. B **18**, 2365 (1985).

[32]An adequate theory that accounts even for the case $\Delta_E = 0$ is much more complicated and requires, e.g., a detailed knowledge of the pressure dependence of the homogeneous optical linewidth in order to evaluate the integrals (3.12) and (3.21).

[33]Y. H. Zou and N. Bloembergen, Phys. Rev. A **33**, 1730 (1986), and references therein.

[34]C. W. Allen, *Astrophysical Quantities,* 2nd ed. (University of London Press, London, 1963), p. 45; the radius of the Sm atom was derived from the lattice constant of solid Sm, C. Kittel, *Introduction to Solid State Physics,* 5th ed. (Wiley, New York, 1976).

[35]J. L. LeGouët, J. Phys. B **11**, 3001 (1978).

[36]M. Borenstein and W. E. Lamb, Jr., Phys. Rev. A **5**, 1311 (1972).

[37]P. R. Berman, J. E. M. Haverkort, and J. P. Woerdman, Phys. Rev. A **34**, 4647 (1986).

[38]P. R. Berman, T. W. Mossberg, and S. R. Hartmann, Phys. Rev. A **25**, 2550 (1982).

[39]M. Gorlicki, A. Peuriot, and M. Dumont, J. Phys. Lett. **41**, L275 (1980).

[40]C. G. Aminoff, J. Javaneinen, and M. Kaivola, Phys. Rev. A **28**, 722 (1983).

[41]X. Zhu, Phys. Rev. A **33**, 251 (1986).

[42]C. Parigger, P. Hannaford, and W. J. Sandle, Phys. Rev. A **34**, 2058 (1986).

[43]W. C. Martin, R. Zahlubas, and L. Hagan, Natl. Stand. Ref. Data Ser., Natl. Bur. Stand. (U.S.) Circ. No. 60 (U.S. GPO, Washington, D.C., 1978), p. 162.

[44]A. Omont, Prog. Quantum Electron. **5**, 69 (1977), and references therein.

[45]T. Manabe, T. Yabuzaki, and T. Ogawa, Phys. Rev. A **20**, 1946 (1979); Phys. Rev. Lett. **46**, 637 (1981).